72-11,673

STUCKLESS, John Shearing, 1944-
THE PETROLOGY AND PETROGRAPHY OF THE VOLCANIC SEQUENCE ASSOCIATED WITH THE SUPERSTITION CALDERA, SUPERSTITION MOUNTAINS, ARIZONA.

Stanford University, Ph.D., 1971
Geology

University Microfilms, A XEROX Company, Ann Arbor, Michigan

THIS DISSERTATION HAS BEEN MICROFILMED EXACTLY AS RECEIVED.

Reproduced with permission of the copyright owner. Further reproduction prohibited without permission.

THE PETROLOGY AND PETROGRAPHY OF THE VOLCANIC SEQUENCE ASSOCIATED WITH THE SUPERSTITION CALDERA, SUPERSTITION MOUNTAINS, ARIZONA

A DISSERTATION

SUBMITTED TO THE DEPARTMENT OF GEOLOGY

AND THE COMMITTEE ON THE GRADUATE DIVISION

OF STANFORD UNIVERSITY

IN PARTIAL FULFILLMENT OF THE REQUIREMENTS

FOR THE DEGREE OF

DOCTOR OF PHILOSOPHY

By

John S. Stuckless

June 1971

Reproduced with permission of the copyright owner. Further reproduction prohibited without permission.

I certify that I have read this thesis and that in my opinion it is fully adequate, in scope and quality, as a dissertation for the degree of Doctor of Philosophy.

Robert R. Compton
(Principal Adviser)

I certify that I have read this thesis and that in my opinion it is fully adequate, in scope and quality, as a dissertation for the degree of Doctor of Philosophy.

Marion A. Langhere

I certify that I have read this thesis and that in my opinion it is fully adequate, in scope and quality, as a dissertation for the degree of Doctor of Philosophy.

I certify that I have read this thesis and that in my opinion it is fully adequate, in scope and quality, as a dissertation for the degree of Doctor of Philosophy.

Approved for the University Committee on Graduate Studies:

Dean of Graduate Studies

Reproduced with permission of the copyright owner. Further reproduction prohibited without permission.

PLEASE NOTE:

Some pages have indistinct print. Filmed as received.

UNIVERSITY MICROFILMS.

Reproduced with permission of the copyright owner. Further reproduction prohibited without permission.

PLEASE NOTE:

Several pages contain colored illustrations. Filmed in the best possible way.

UNIVERSITY MICROFILMS

Reproduced with permission of the copyright owner. Further reproduction prohibited without permission.

TABLE OF CONTENTS

	Page
LIST OF TABLES	
LIST OF ILLUSTRATIONS	
ABSTRACT	1
ACKNOWLEDGEMENTS	4
INTRODUCTION	5
STRATIGRAPHY	10
Introduction	10
Precambrian granitic basement	10
Arkosic conglomerate	14
Older basalt	14
Older dacite complex	15
Superstition Tuff	24
Geronimo Head Formation	31
Younger mafic lavas	36
Younger silicic domes and lavas	40
GEOCHRONOLOGY	46
The Precambrian granitic basement	46
The Tertiary volcanic sequence	52
INITIAL SR^{87}/SR^{86} RATIOS AND THEIR IMPLICATIONS	57
Introduction	57
Analytical procedure	58
Results and discussion	59
OXYGEN ISOTOPE DATA	68
ORIGIN OF THE MAGMAS	78
STRUCTURAL EVOLUTION	94
SUMMARY	103
REFERENCES	107

Reproduced with permission of the copyright owner. Further reproduction prohibited without permission.

LIST OF TABLES

Table		Page
1.	Modal analyses for the Precambrian basement	13
2.	Chemical analyses and rock norms	16
3.	Modal data for the mafic lavas	20
4.	Modal data for the silicic domes and lavas	23
5.	Modal data for the pyroclastic rocks	26
6.	Average chemical data for the Superstition Tuff and Apache Leap Tuff	30
7.	Rb-Sr isotope data for the Precambrian basement	48
8.	Fission-track ages	49
9.	K-Ar data and ages	53
10.	Initial Sr^{87}/Sr^{86} ratios and Rb/Sr ratios	60
11.	Oxygen isotope measurements	69
12.	Oxygen isotope temperature determinations	70
13.	Partial chemical analyses of minerals	76
14.	Experimental and hypothetical data	85

Reproduced with permission of the copyright owner. Further reproduction prohibited without permission.

LIST OF ILLUSTRATIONS

Figure		Page
1.	Index map to the Superstition area	6
2.	Idealized stratigraphic section.	11
3.	Photograph of the older dacite with inclusions . . .	22
4.	Photograph of the Superstition Tuff.	28
5.	Photograph of Geronimo Head.	33
6.	Photograph of Geronimo Head lahars	34
7.	Photograph of Black Mesa and Black Top Mesa.	37
8.	Photograph of flow-banded quartz latite lava	43
9.	Photomicrograph of remelted plagioclase.	44
10.	Photograph of intrusive dome at Apache Gap	55
11.	The variation of O^{18} in plagioclase phenocrysts. . .	72
12.	Oxygen isotope fractionation curves.	74
13.	Silica variation diagrams.	79
14.	The system Q-Or-Ab	89
15.	Photograph of the ring fracture zone of the Black Mesa cauldron.	100

Plate

1.	Geologic Map of the Superstition Mountain Area . . .	In pocket

Reproduced with permission of the copyright owner. Further reproduction prohibited without permission.

ABSTRACT

Three periods of igneous activity are recorded in the rocks of the Superstition Mountain region. Two plutonic events occurred in the Precambrian (about 1650 m.y. and 1400 m.y.), and a volcanic event occurred in the middle Tertiary. The Tertiary volcanism started with the extrusion of a thin alkali olivine basalt over an arkosic conglomerate. This was followed by the intrusion and extrusion of a ring of dacite domes (29 m.y.). The early dacites were quartz-poor and were followed by more voluminous "normal" dacites.

The last phases of dacite volcanism were accompanied by the eruption of the Siphon Draw Member of the Superstition Tuff (24.4 m.y.). The eruption of this tuff is believed to have been contemporaneous with caldera collapse because of the thick accumulation of tuff within the caldera.

The first ash flows of the Geronimo Head Formation were erupted either during the last phases of collapse or shortly thereafter. These ash flows were accompanied by an alkali olivine basalt and were closely followed by the extrusion and intrusion of quartz latite domes and lavas (20 m.y. and 21 m.y.). Resurgence of the quartz latite magma up-domed the central core of the Superstition caldera.

A similar volcanic cycle started with the eruption of the Dogie Spring Member of the Superstition Tuff (18.4 m.y.). This was followed by more rhyolite ash flows of the Geronimo Head Formation (16.3 m.y.),

Reproduced with permission of the copyright owner. Further reproduction prohibited without permission.

a basanite lava (17 m.y.) and more quartz latite lavas and domes (16.1 m.y.).

Several smaller cauldrons were formed during this period: The Willow Springs cauldron, the Black Mesa cauldron, and the Florence Junction cauldron. Various episodes of magma resurgence up-lifted the central core of each cauldron and formed domes within the ring fracture zone of the Superstition caldera.

Volcanism came to a close between 10 and 15 million years ago. The Canyon Lake Member of the Superstition Tuff (15 m.y.) appears to be the last ash flow and was closely followed by the extrusion of a thin alkali olivine basalt. The final volcanic event appears to have been the emplacement of small rhyolite dikes and domes around the outer margin of the Superstition caldera.

Strontium isotope studies indicate that the magma (s) for the Superstition volcanics must have been derived below the base of the granitic crust. Both the silicic and mafic volcanics have similar, relatively low initial Sr^{87}/Sr^{86} ratios. They may therefore be related to a common source. It is proposed that the magmas were derived by fractional fusion of the lower crust. Once formed, the magmas differentiated independently forming two suites which are discontinuous with one another but cogenetic.

Most of the volcanics started to crystallize at high temperatures and pressures as indicated by the system Q-Or-Ab-H_2O and oxygen isotope geothermometry. The magmas were undersaturated with respect to water. During ascent to the surface the magmas underwent minor crystal-melt re-equilibration and cooled. This cooling was accompanied by the crystallization of biotite. Prior to eruption the upper portions of the

Reproduced with permission of the copyright owner. Further reproduction prohibited without permission.

magma column assimilated Sr^{87} from the granitic basement such that the base of each quartz latite ash flow is now enriched in Sr^{87}.

The magma responsible for the Geronimo Head Formation appears to have had a much longer time of residence in the crust at lower pressures and temperatures than the rest of the magmas. This is indicated by its greater enrichment in Sr^{87}, lower oxygen isotope temperatures, and liquidus composition in the system Q-Or-Ab-H_2O. These conditions suggest that the magma chamber associated with the collapse features had a depth of 2 to 5 km.

Reproduced with permission of the copyright owner. Further reproduction prohibited without permission.

ACKNOWLEDGEMENTS

The writer wishes to acknowledge financial support from Arizona State University Graduate Teaching Assistant Research Program and Arizona State University Faculty Research Grant 5271-285. Parts of this project were supported by a Sigma Xi grant-in-aid-of-research and by the Shell Research Fund at Stanford University.

Several persons have contributed greatly to this project. The writer is indebted to M.A. Lanphere, S.C. Creasy, Jr. R. O'Neil and C.W. Naeser who made their laboratories and time available. This study has benefited greatly from the guidance of R.R. Compton, W.C. Luth, N. Page and M.F. Sheridan. The writer also wishes to thank M.L. Silberman for K/Ar age determinations and several helpful discussions.

Reproduced with permission of the copyright owner. Further reproduction prohibited without permission.

INTRODUCTION

The Superstition caldera is located in the Superstition Wilderness Area, approximately 60 kilometers east of Phoenix, Arizona (fig. 1). The area of study consists of approximately 500 square kilometers of largely volcanic terrain which is part of a larger volcanic complex.

This volcanic complex is composed mainly of silicic ash-flow tuffs, lavas, epiclastic breccias, and moderate-size domes. Most of the volcanics rest directly on the Precambrian granitic basement, but locally they rest on a thin Miocene arkosic conglomerate or on remnants of Precambrian metamorphic rocks.

The Tertiary ash-flow fields of the western United States have recently gained wide recognition. Much of the recent emphasis on the quantitative importance of ash-flow tuffs is due to the work of Mackin (1960, p. 83) who estimated the volume of ash-flow tuffs in western North America at 4×10^5 cubic kilometers. Peterson (1970) has stressed the importance of ash flows in regional stratigraphy, structural interpretation and the understanding of igneous processes.

Throughout the world and particularly in the western United States, an intensive search has been started to find the eruptive centers for these extrusives. Eruptive centers for ash volumes of a few cubic kilometers or more are thought to be either collapse calderas or volcano-tectonic depressions (Smith, 1960, p. 818).

Reproduced with permission of the copyright owner. Further reproduction prohibited without permission.

Reproduced with permission of the copyright owner. Further reproduction prohibited without permission.

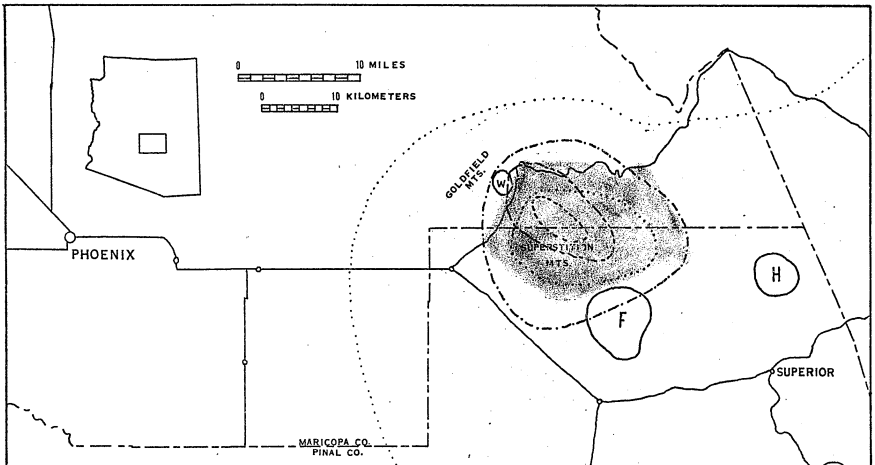

Figure 1 - Index map to the Superstition - Superior volcanic area showing the distribution of volcano-tectonic collapse features. The western limits of the volcanic field are shown by the light dotted line. The approximate limits of collapse for the Willow Springs, Florence Junction and Haunted Canyon Cauldrons are shown by solid lines and are marked (W), (F), and (H) respectively. The maximum limit of collapse for the Black Mesa Cauldron is shown by the dash-bar line, and its resurgent core is shown by a dashed line. The maximum limit of collapse for the Superstition Caldera is shown by a dot-dash line and its resurgent core is shown by a heavy dotted line. The area mapped in Plate 1 is shown by shading.

These collapse structures range in size from 2 to 140 kilometers in diameter.

Collapse calderas with structural motif and rock suites similar to those identified in this study have been described in several regions adjacent to the Colorado Plateau. Four of the best known are: the Creede caldera in the San Juan Mountains, Colorado (Ratte and Steven, 1967); the Silverton and Lake City calderas also in the San Juan Mountains (Luedke and Burbank, 1968); the Valles in the Jemez Mountains, New Mexico (Smith, and others, 1961); and the Timber Mountain caldera north of Las Vegas, Nevada (Christiansen and others, 1965).

Studies along the eastern margin of the Superior-Superstition volcanic area (fig. 1) have indicated a caldera in Haunted Canyon (Peterson, 1961). Studies in the western part of this volcanic area have shown the region to be a complex volcanic source area consisting of the Willow Springs cauldron (Sheridan, 1968), the Black Mesa cauldron (Sheridan and Stuckless, 1969) and the Superstition caldera (Sheridan, Stuckless and Fodor, 1970). A possible fourth cauldron may be located just north of Florence Junction.

Volcano-tectonic collapse features suggest relatively shallow magma chambers. In the Superstition region the host rock for a shallow magma chamber would be the Precambrian granitic basement. This basement has become greatly enriched in Sr^{87}, and therefore its contribution to magma generation can be estimated by the study of strontium isotopes in the volcanic rocks. This is especially true because the only other probable source materials (the lower crust and mantle) should have relatively low Sr^{87}/Sr^{86} ratios (Doe, 1968).

Reproduced with permission of the copyright owner. Further reproduction prohibited without permission.

Only limited geologic mapping has been done in the Superior-Superstition volcanic area. The Arizona Geologic Map (Wilson, and others, 1969) shows the Superior-Superstition volcanic areas as chiefly undifferentiated Tertiary volcanics. The Goldfield Mountains (fig. 1) are composed primarily of rhyolite ash flows and silicic lavas (Sheridan and Fodor, 1968). Farther east in the Superstition Wilderness Area, the volcanic sequence is dominated by welded quartz latite tuffs (Stuckless, 1969).

The terminology used in this paper follows that proposed by Smith (1960) and Ross and Smith (1961) for ash-flow tuffs and that of Fisher (1960) for breccias. The term cauldron is used for the smaller irregularly shaped volcano-tectonic depressions. The term caldera is used for the larger nearly circular volcano-tectonic depressions. The stratigraphic units reported in this study are compatible with those reported by Sell (1968) for the volcanic belt extending 176 kilometers from Globe to Gila Bend.

Because little detailed geologic information is available for the Superstition Wilderness Area, the first objectives of this report are: 1) To describe the stratigraphy and lithologic units; 2) to report the geochronology; and 3) to present new evidence relating to the Superstition caldera. The second part of this report will be concerned with the interpretation of petrographic, chemical, strontium isotope and oxygen isotope data.

These data suggest complex magma history. The first stage is one of partial fusion in the lower crust to form an intermediate to silicic magma. This magma then started to crystallize and differentiate before moving into the upper crust. The majority of the magma erupted

Reproduced with permission of the copyright owner. Further reproduction prohibited without permission.

following a relatively short period of residence in a shallow magma chamber. Some of the magma appears to have had a longer period of crustal residence. During this time the magma underwent further differentiation and became contaminated with crustal strontium.

Reproduced with permission of the copyright owner. Further reproduction prohibited without permission.

STRATIGRAPHY

Introduction

The stratigraphic sequence in the Superstition Wilderness Area includes volcanic rocks ranging from basanite (43% SiO_2) to rhyolite (72% SiO_2). However, rocks containing 49% to 59% silica are apparently absent. The eruptive types exhibit a wide variation including massive lava flows, autoclastic flow breccias, epiclastic breccias, ash-flow tuffs and flow-banded domes. With the exception of the lack of andesites, the stratigraphic sequence reported here (fig. 2) is similar to the Tertiary sequence found elsewhere in the Basin and Range Province of Arizona: 1) arkosic conglomerate; 2) basalt and/or andesite lava; 3) quartz latite and/or rhyolite ash-flow tuffs; 4) rhyolite epiclastic breccias, and/or late basalts. This sequence is essentially Ransome's (1903) classic andesite-rhyolite-basalt stratigraphy for southwestern volcanic fields. Examples of this sequence are numerous: Santa Cruz County - The Chiricahua Mountains (Marjaniemi, 1968, Fernandez and Enlows, 1966); Pima County - The Roskrüge Mountains (Bickerman, 1968), The Tucson Mountains (Mayo, 1968); and Pinal County - Gila Bend to Superior (Sell, 1968), Picket Post Mountain (Peterson, 1966), and The Galiuro Mountains (Krieger, 1968).

Precambrian Granitic Basement

The oldest rocks of the area studied are quartz monzonites of

Reproduced with permission of the copyright owner. Further reproduction prohibited without permission.

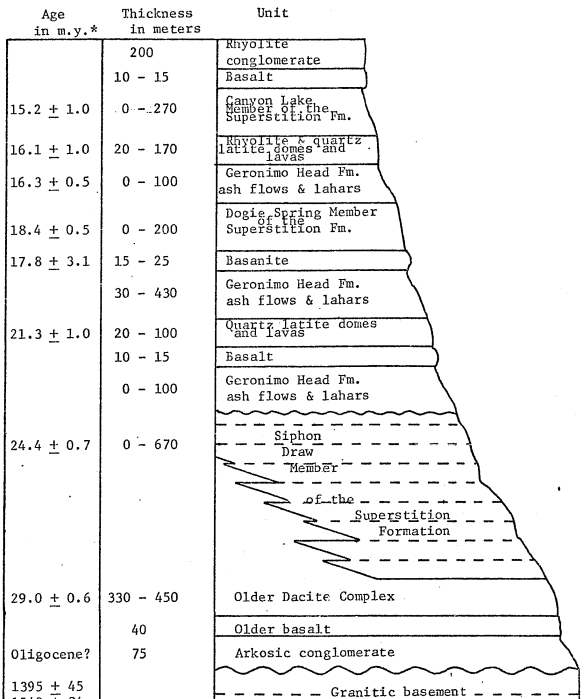

Figure 2 - Idealized stratigraphic section for the Superstition Mountain region. Age determination data are listed in tables 7, 8 and 9.

Reproduced with permission of the copyright owner. Further reproduction prohibited without permission.

Precambrian age. These crop out along most of the circumference of the Superstition caldera (plate 1), but are buried along the northwestern margin. The quartz monzonites collected at the northeastern margin of the caldera are correlated with the Ruin granite. They are typically coarse-grained with large phenocrysts of orthoclase (5 cm) and contain less than 10% mafic minerals (table 1). Similar rocks used in this study were collected northwest of the caldera along Highway 87.

The quartz monzonites along the southern and southwestern margins of the caldera are slightly foliated and coarsely equigranular. The rocks generally contain greater than 10% mafic minerals (table 1) and locally contain mafic segregations. These quartz monzonites are tentatively correlated with the Madera quartz diorite.

The quartz monzonites are generally weathered and decomposed. Prospects with shafts up to 20 meters in depth often expose no fresh rock and within the area studied relief in the Precambrian basement is generally low and exposures are poor. For these reasons many of the basement samples analysed in this study were collected outside of the area mapped.

Other features observed in the Precambrian basement include a few linear zones (up to 10 meters wide) which trend northeastward and east-west. These zones are best displayed along the southwestern margin of the caldera and consist of well-cemented breccias, aplite dikes and coarsely crystalline orthoclase in a chlorite and clay matrix. Along the eastern margin the Precambrian rocks are predominantly large fault blocks of metamorphics.

Reproduced with permission of the copyright owner. Further reproduction prohibited without permission.

TABLE 1

MODAL ANALYSES FOR THE PRECAMBRIAN GRANITIC BASEMENT[a]

Sample No.[b]	Unit[c]	Quartz	Plagioclase	Potassium feldspar	Mafic
7133	1?	23.2	34.0	22.7	20.2
7134	1?	16.5	27.7	39.2	16.7
7136	1?	18.7	31.0	32.0	18.3
7230	1?	31.5	27.3	25.2	16.0
7272	1?	20.0	41.6	26.0	12.4
7321	1?	22.0	29.8	19.3	28.8
8144	1	21.3	25.1	35.1	18.5
AP-209	1	44.0	30.2	19.6	6.2
AP-211	1	23.5	40.0	9.5	26.0
AP-231	1	37.8	24.2	35.2	2.8
7105	2?	32.7	28.9	30.2	8.2
7106	2?	20.3	33.7	40.2	5.8
8145	2	30.6	34.7	31.1	3.6
AP-201	2	33.8	47.8	26.6	2.0

a. Determined by point counting 500 or more points on a stained slab. Samples AP-209 and AP-211 point counted in thin section.

b. Data for Samples in 7000 Series from Kokalis (1971). Data for Samples in 8000 Series from Sheridan (1970, written communication).

c. 1 = older Precambrian (Madera Quartz Diorite)
2 = younger Precambrian (Ruin Granite)
? = assignment uncertain.

Reproduced with permission of the copyright owner. Further reproduction prohibited without permission.

Arkosic Conglomerate

The quartz monzonite is non-conformably overlain by an arkosic sandstone and conglomerate sequence. Erosion has removed much of this unit which is mainly preserved as down-dropped fault blocks in the quartz monzonite.

This unit varies from a moderately well-sorted arkosic sandstone to a poorly sorted boulder conglomerate. The clasts, which range up to one meter in diameter, consist of Precambrian granite, schist, quartzite and Paleozoic limestone. The colors range from dusky red for the conglomerate to a dark red for the sandstone. In thin section the arkosic sandstone exhibits one to two millimeters angular clasts of quartz, plagioclase, perthitic orthoclase, microcline, muscovite and various oxidized mafics, some of which show euhedral amphibole outlines.

Within the Goldfield and Superstition regions the arkosic sequence attains a maximum thickness of 72 meters. This unit is tentatively correlated with the White Tail conglomerate of the Superior region which is believed to be Oligocene in age (Banks, personal communication, 1971).

Older Basalt

Directly overlying the arkose and apparently interbedded with it west of the area mapped is an alkali-olivine basalt which attains a maximum thickness of 40 meters. Locally the unit is composed of two flows separated by a light colored ash and/or basaltic breccia midway in the section. The basalt flows were apparently extensive enough to have once covered most of the Superstition area, but now exist only as remnants around the caldera periphery. Possible vents are

Reproduced with permission of the copyright owner. Further reproduction prohibited without permission.

located at Government Wells and just south of the J.F. Ranch, where the basalt reaches its maximum thickness (plate 1).

The older basalt varies in color from grey to dark grey with red phenocrysts of iddingsite. In areas of low relief, it is generally exposed as a rubbly surface. At Government Wells the flow contains large, much altered mafic nodules.

Textures observed in thin section vary from intergranular to diabasic. Chemical, normative, and modal data for this unit are reported in tables 2 and 3. Normative nepheline greater than 0 but less than 5% and modal olivine greater than 5% classify this unit as an alkali-olivine basalt (Wilkinson, 1967, p. 167).

Older Dacite Complex

The older dacite crops out along a roughly semicircular arc around the Superstition caldera. The dacite attains a thickness of at least 450 meters. The unit is largely composed of dacitic domes and associated autobrecciated lava flows. Considerable relief resulted from emplacement of the domes, as shown by the fact that the overlying welded tuff rapidly pinches out against the flanks of several domes.

The older dacite complex is composed of rocks ranging in composition from near andesite (quartz-rich) to near quartz latite and appears to have a general trend of increasing silica with time. The quartz-poor dacite is dark grey with mafic phenocrysts altering to red iron oxides, though in a few places, apparently where it is freshest, it is a light olive-grey. The quartz-poor dacite occurs only in small dikes or flows near the base of the large domes and is not found associated with the more extensive auto-brecciated flows

Reproduced with permission of the copyright owner. Further reproduction prohibited without permission.

Reproduced with permission of the copyright owner. Further reproduction prohibited without permission.

TABLE 2

ANALYSES FOR MAJOR OXIDES BY WEIGHT PERCENT[1] AND ROCK NORMS[2]

Sample number[3]	Older basalt 8068	Older 8092[4]	Dacite 8095[4]	Complex 8114	Siphon 8074	Draw AP-232	Member AP-236	Geronimo Head Formation 8103	Geronimo Head Formation AP-215	Dogie Spring Member AP-205
SiO_2	49.88	59.53	60.42	63.62	69.87	71.0	71.4	70.96	68.19	70.2
TiO_2	1.08	0.93	1.05	0.69	0.50	0.42	0.42	0.16	0.15	0.42
Al_2O_3	15.97	17.15	16.86	18.09	14.61	14.6	14.0	12.14	11.4	14.5
Fe_2O_3	6.98	4.75	4.65	1.36	2.65	2.0	2.1	1.31	0.48	1.8
FeO	0.82	0.57	0.64	0.66	0.38	0.52	0.48	0.20	0.36	0.52
MgO	7.11	2.46	1.95	1.83	0.81	0.73	0.49	0.56	0.35	0.65
MnO	0.18	0.07	0.06	0.09	0.09	0.04	0.09	0.07	0.04	0.07
CaO	8.51	4.63	4.33	2.29	1.97	1.8	1.6	1.09	2.8	1.8
Na_2O	3.89	4.36	4.35	4.32	3.68	3.5	3.8	1.39	1.1	3.9
K_2O	2.13	2.62	2.91	3.46	3.82	4.0	4.0	5.63	3.5	4.0
H_2O+	2.14	1.69	1.71	2.12	0.83	0.92	0.83	3.14	6.2	1.1
H_2O^-	1.25	0.99	0.84	1.09	0.40	0.38	0.47	3.03	4.6	0.83
P_2O_5	0.08	0.31	0.46	0.41	0.04	0.16	0.12	0.04	0.02	0.11
Total	100.02	100.06	100.23	100.03	99.65	100.	100.	99.72	100.	100.
Q	0.0	12.06	13.67	19.39	28.39	30.83	30.23	40.91	42.64	27.72
C	0.0	0.0	0.0	4.19	0.95	1.62	0.80	2.00	0.76	0.75
Or	13.03	15.90	17.64	21.12	22.94	23.63	23.68	35.56	20.70	23.66
Ab	29.90	37.89	37.75	37.76	31.64	29.60	32.22	12.57	9.31	33.03
An	20.52	20.01	17.84	8.97	9.67	7.88	7.17	5.50	13.77	8.22
NE	2.26	0.0	0.0	0.0	0.0	0.0	0.0	0.0	0.0	0.0
WO	9.45	0.30	0.06	0.0	0.0	0.0	0.0	0.0	0.0	0.0
EN	8.17	6.29	4.98	4.71	2.05	1.82	1.22	1.49	0.87	1.62
FS	0.0	0.0	0.0	0.0	0.0	0.0	0.0	0.0	0.0	0.0
FO	7.12	0.0	0.0	0.0	0.0	0.0	0.0	0.0	0.0	0.0
Fa	0.0	0.0	0.0	0.0	0.0	0.0	0.0	0.0	0.0	0.0
MT	0.10	0.0	0.0	0.44	0.07	0.68	0.63	0.44	0.70	0.69
HM	7.15	4.88	4.77	1.11	2.64	1.53	1.67	1.10	0.0	1.33
AP	0.20	0.75	1.12	1.00	0.10	0.38	0.29	0.10	0.05	0.26
IL	2.12	1.39	1.52	1.35	0.97	0.74	0.80	0.33	0.29	0.80

Reproduced with permission of the copyright owner. Further reproduction prohibited without permission.

TABLE 2--Continued

Sample	Canyon	Lake	Member	Black Mesa Basanite		Willow Springs Basalt	Rhyolite Domes	
number	8086	AP-234	AP-235	8062	8102	8070	8011	AP-27a
SiO_2	68.98	69.0	67.9	43.33	43.51	46.92	71.07	72.6
TiO_2	0.41	0.44	0.45	1.31	1.35	1.69	0.14	0.24
Al_2O_3	14.59	15.2	15.1	17.20	17.01	15.41	13.29	13.1
Fe_2O_3	2.50	2.2	2.2	5.73	6.96	4.79	0.85	0.52
FeO	0.25	0.40	0.44	4.29	3.36	4.89	0.62	0.80
MgO	0.71	0.75	0.77	6.73	6.89	9.17	0.14	0.38
MnO	0.09	0.05	0.09	0.19	0.20	0.15	0.04	0.04
CaO	1.20	1.9	2.4	13.63	13.78	8.74	0.23	1.2
Na_2O	2.41	3.6	3.0	3.68	3.53	3.25	3.09	4.0
K_2O	6.48	4.2	4.8	0.88	0.94	1.97	5.07	3.9
H_2O^+	1.58	1.1	1.2	1.84	1.49	1.93	4.46	3.7
H_2O^-	0.49	0.79	1.2	0.21	0.13	0.28	0.66	0.27
P_2O_5	0.20	0.12	0.16	0.62	0.69	0.48	0.05	0.16
Total	99.89	100.	100.	99.64	99.84	99.67	99.71	100.
Q	27.70	27.20	26.31	0.0	0.0	0.0	34.89	31.11
C	1.95	1.57	0.99	0.0	0.0	0.0	2.56	0.50
Or	39.15	24.88	28.45	5.33	5.57	11.95	31.67	22.84
Ab	20.85	30.54	25.46	8.75	9.30	23.08	27.64	33.54
AN	4.75	8.66	10.89	28.50	27.87	22.21	0.86	4.86
NE	0.0	0.0	0.0	12.55	11.19	2.79	0.0	0.0
WO	0.0	0.0	0.0	15.30	15.10	7.96	0.0	0.0
EN	1.81	1.87	1.92	12.47	13.05	6.35	0.37	0.94
FS	0.0	0.0	0.0	0.99	0.0	0.70	0.30	0.71
FO	0.0	0.0	0.0	3.30	2.91	11.97	0.0	0.0
Fa	0.0	0.0	0.0	0.29	0.0	1.45	0.0	0.0
MT	0.0	0.18	0.41	8.51	7.59	7.13	1.30	0.75
HM	2.56	2.08	1.92	0.0	1.75	0.0	0.0	0.0
AP	0.48	0.28	0.38	1.50	1.64	1.17	0.13	0.38
IL	0.74	0.84	0.86	2.55	2.57	3.29	0.28	0.45

Reproduced with permission of the copyright owner. Further reproduction prohibited without permission.

TABLE 2--Continued

Sample number	Quartz latite domes & dikes						Quartz latite lavas	
	8073	7486	AP-219	AP-213	AP-212	AP-217	8067	8125
SiO_2	64.60	65.33	66.8	67.2	71.2	72.1	68.28	70.96
TiO_2	0.51	0.49	0.61	0.44	0.41	0.26	0.44	0.33
Al_2O_3	15.72	15.25	14.5	15.0	14.5	14.2	14.74	13.93
Fe_2O_3	1.97	1.65	2.0	1.8	1.7	1.8	0.87	0.77
FeO	0.97	1.68	0.80	1.1	0.6	0.44	1.53	0.94
MgO	1.14	0.85	0.87	1.0	0.7	0.61	0.56	0.31
MnO	0.06	0.09	0.06	0.05	0.07	0.02	0.09	0.05
CaO	2.67	2.45	2.3	2.9	2.0	1.7	2.81	1.22
Na_2O	3.91	4.09	3.6	3.8	3.2	3.2	3.51	3.16
K_2O	3.73	3.22	2.8	3.4	4.1	4.2	4.23	4.59
H_2O^+	3.48	3.96	4.6	2.5	0.83	1.1	3.06	2.71
H_2O^-	1.14	0.72	0.88	0.36	0.67	0.3	0.05	0.57
P_2O_3	0.04	0.17	0.05	0.16	0.11	0.16	0.11	0.09
Total	99.94	99.95	100.	100.	100.	100.	100.28	99.63
Q	21.27	22.87	20.10	24.90	31.85	33.28	25.42	33.11
C	0.52	1.00	1.49	0.18	1.42	1.68	0.0	1.83
Or	23.12	19.18	15.57	20.15	24.21	24.80	25.72	28.15
Ab	34.71	34.88	30.50	32.25	27.05	27.05	30.57	27.75
AN	13.62	11.13	11.10	13.38	9.20	7.38	12.32	5.67
NE	0.0	0.0	0.0	0.0	0.0	0.0	0.0	0.0
WO	0.0	0.0	0.0	0.0	0.0	0.0	0.54	0.0
EN	2.98	2.13	2.17	2.50	1.74	1.52	1.44	0.80
FS	0.0	1.09	0.0	0.0	0.0	0.0	1.58	0.66
FO	0.0	0.0	0.0	0.0	0.0	0.0	0.0	0.0
Fa	0.0	0.0	0.0	0.0	0.0	0.0	0.0	0.0
MT	1.93	2.41	1.01	2.44	0.97	0.73	1.30	1.16
HM	0.73	0.0	1.31	0.12	1.03	1.30	0.0	0.0
AP	0.10	0.41	0.12	0.38	0.26	0.38	0.27	0.22
IL	1.02	0.94	1.16	0.84	0.78	0.49	0.86	0.65

TABLE 2--Continued

Explanation for Table 2:

1. 7000 and 8000 series numbers analyzed by H. Onuki, Tohoku University, Japan. AP series numbers analyzed by x-ray fluorescence supplemented by methods described in U.S. Geological Survey Bulletin 1144-A. Analysts: P. Elmore, G. Chloe, H. Smith, J. Glenn, and J. Kelsey.

2. Norms calculated by computer program no. C128, U.S. Geological Survey.

3. Sample locations shown on plate 1.

4. Samples of quartz-poor dacite.

Reproduced with permission of the copyright owner. Further reproduction prohibited without permission.

TABLE 3

MODAL DATA FOR THE MAFIC LAVAS

Sample No.	% Phenocrysts	Plagioclase	Olivine	Augite	Nepheline	Opaques
8068[1]	15.2		19.5	46.7		33.8
AP-243[1]	7.6	tr	65.8	28.9		5.3
2	14.8 ±1.07		59.4 ±5.2	27.7 ±1.5		14.8 ±6.6
3	11.1 ±1.3		19.0 ±0.9	55.0 ±2.9	14.8 ±3.9	11.2 ±5.9
4	8.6 ±1.0	65.1 ±4.3	17.2 ±2.1	16.8 ±1.9		0.82 ±0.21

1. Older basalt.
2. Willow Springs basalt, average of 3 Samples ±1 σ .
3. Black Mesa Basanite, average of 5 Samples ±1 σ .
4. Canyon Lake basalt, average of the wholerock for two Samples ±1 σ . The phenocrysts are entirely olivine.

Reproduced with permission of the copyright owner. Further reproduction prohibited without permission.

of quartz-rich or normal dacite. In a few places the older dacite domes contain abundant inclusions of the older rocks as well as cognate inclusions (fig. 3). These areas are interpreted as vents.

The rocks referred to as normal dacites comprise an estimated 95% of the older dacite complex, occurring as flow-banded domes and auto-brecciated lava flows. The flow-banded rocks are reddish-grey with thin red bands. The autobrecciated lavas are distinguished by rubbly weathering and a light brown color.

An extensive area in the southwestern portion of the area mapped has been strongly altered to a white rock with little or no megascopic texture. This rock is included with the older dacite complex on the basis of faint outlines of original texture similar to that of the domes. These ghost textures may usually be observed only in thin section.

The two dacitic types which make up the older dacite complex are easily distinguished in thin section (table 4). The normal dacite generally has a greater percentage of phenocrysts (30% as opposed to 24%) and a greater percentage of phenocrysts are plagioclase (69% versus 50%). The quartz-poor dacite has hornblende as its dominant mafic (about 25% of the phenocrysts) and more augite than the normal dacite (8.8% versus a trace). Both dacitic types generally exhibit trachytic texture; however, some samples of the normal dacite have spherulitic devitrification textures and intergrowths of quartz and plagioclase indicating that these were once glassy rocks. The plagioclase composition in the normal dacites was found to vary between An_{32} in the core to An_{25} at the rim by using the universal stage determination curves of Slemmons (1962).

Reproduced with permission of the copyright owner. Further reproduction prohibited without permission.

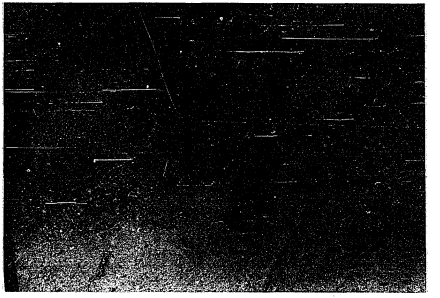

Figure 3 - Older dacite dome with abundant inclusions. The large partially resorbed block is a basalt inclusion.

Reproduced with permission of the copyright owner. Further reproduction prohibited without permission.

TABLE 4

MODAL DATA FOR THE SILICIC DOMES AND LAVAS

Sample No.	% Phenocrysts	Quartz	Plagioclase	Sanidine	Biotite	Hornblende	Augite	Sphene	Opaques
1	24.3 ±3.5	tr	50.2 ±3.4	-	tr	25.2 ±6.9	8.8 ±5.8	-	7.3 ±3.8
2	30.1 ±7.5	4.4 ±4.3	68.9 ±2.0	tr	6.5 ±4.9	12.0 ±5.6	tr	-	7.3 ±7.8
3	28.8 ±6.4	2.5 ±2.9	71.6 ±7.4	tr	4.4 ±4.1	15.9 ±5.4	-	tr	4.4 ±4.1
4	32.2 ±4.9	40.6 ±16.0	41.3 ±17.3	5.1 ±5.4	9.8 ±12.5	1.1 ±0.9	-	tr	1.6 ±0.8
5	3.3 ±1.6	1.9 ±2.5	71.2 ±11.0	-	13.5 ±9.2	7.3 ±7.4	tr	tr	2.5 ±2.5

1 - Quartz poor dacite, average of 3 samples ±1 σ

2 - Normal dacite, average of 8 samples ±1 σ

3 - Quartz latite domes and lavas - group 1, average of 12 samples ±1 σ

4 - Quartz latite domes and lavas - group 2, average of 5 samples ±1 σ

5 - Rhyolite domes, average of 4 samples ±1 σ .

Reproduced with permission of the copyright owner. Further reproduction prohibited without permission.

The classification of quartz-poor dacite is based on chemical and normative data (table 2). Comparison of these chemical data with that of Barth (1962, p. 58) for average effusive rocks shows that the quartz-poor dacite is low in silica relative to Barth's average dacite, but high relative to Barth's average andesite.

If the rock is classified on the basis of modal mineralogy by plotting the mode on Rittmann's classification diagram (1962, p. 98), the rock is an andesite. Although chemical data and observed rock textures are in accord with this classification, the normative data are not. Using O'Conner's (1965, B-82) normative feldspar classification for rocks containing greater than 10% quartz, these rocks would be rhyodacites. Tabor and Crowder (1969, p. 28) have reclassified several Cascade andesites as dacites based on normative quartz, plagioclase and orthoclase. Because the dacitic rocks from the Superstitions contain greater than 10% normative quartz, and because plagioclase constitutes two-thirds of the total feldspar, the rocks fall into the lower limits of the dacite field and are therefore called quartz-poor dacites.

The rocks from the older dacite complex referred to as normal dacites are classified on the basis of modal mineralogy and by comparison with the quartz-poor dacites. By strict modal classification these rocks would be classified as andesites; however, because they contain more quartz than the quartz-poor dacite, rock norms for this unit would undoubtedly show them to be normal dacites.

The Superstition Tuff

A sequence of welded quartz-latite tuffs was erupted during the last stages of dacite volcanism. These are divided into three members

Reproduced with permission of the copyright owner. Further reproduction prohibited without permission.

on the basis of modal mineralogy (table 5): The Siphon Draw Member, the Dogie Spring Member, and the Canyon Lake Member. Within the Superstition area the three members display all degrees of welding and are always devitrified. The colors of these tuffs darken with intensity of welding ranging from pinkish grey to pale red. The densely welded tuffs (porosity less than 10%) form massive cliffs in which columnar joints are often developed. In these exposures pumice fragments are generally flattened such that the ratio of their height to length is about 1 to 10.

The partially welded tuff (porosity between 10% and 45%) is usually a slope-former. The rock has a lower crystal content than the densely welded tuff and exhibits large, apparently undeformed pumice fragments (up to six centimeters in diameter) with a length to height ratio of about 2 to 1. Both the pumice shape and crystal percentage are attributed to a lesser degree of compaction. Compaction reduces the pore space which means that a given number of crystals occupy a smaller volume thereby raising the apparent volumetric percentage.

When viewed in thin section the Superstition Tuff has typical welded tuff textures although much of the detail has been obscured by devitrification. The densely welded specimens exhibit flattened pumice and tricuspate shards. Quartz is clear, deeply embayed and often shows undulatory extinction. Sanidine is usually clear and forms large euhedral to subhedral crystals which are often twinned according to the Carlsbad or Baveno laws. Plagioclase is generally subhedral with a $2V_x$ of about 80^o indicating an average composition of An_{30}. Universal stage determinations by the Federow technique (Slemmons, 1962) and by the zonal technique (Burri, Parker and Wenk, 1967) showed that

Reproduced with permission of the copyright owner. Further reproduction prohibited without permission.

TABLE 5

MODAL DATA FOR THE PYROCLASTIC ROCKS

Sample No.	% Phenocrysts	Quartz	Plagioclase	Sanidine	Biotite	Hornblende	Sphene	Augite	Opaques
1	41.5 ±5.8	46.9 ±2.8	34.0 ±2.3	10.7 ±2.0	4.5 ±2.6	1.4 ±1.0	0.6 ±0.5	-	2.1 ±1.3
2	28.7 ±9.4	44.4 ±2.6	26.1 ±1.6	21.4 ±0.8	5.3 ±2.3	tr	tr	-	2.5 ±0.5
3	30.2 ±12.5	36.9 ±2.4	39.6 ±3.3	13.4 ±2.1	8.6 ±1.1	-	1.0 ±0.4	-	2.9 ±2.9
4	9.8 ±1.8	35.4 ±9.6	24.8 ±8.0	26.9 ±4.4	6.1 ±5.9	tr	tr	tr	3.3 ±3.0
5	20.0 ±12.7	35.9 ±7.2	21.1 ±4.0	24.8 ±4.9	6.7 ±6.2	2.1 ±1.9	2.3 ±2.0	tr	5.5 ±4.7
6	41.89 ±1.50	18.99 1.84	59.63 1.36	10.13 1.18	8.09 1.05	tr	tr	-	2.23 0.63
7	32.6 ±3.7	14.3 ±2.4	58.0 ±2.6	11.7 ±3.0	8.8 ±1.9	6.9 ±0.9	tr	-	1.1 ±0.7
8	39.2	10.8	71.4	3.4	8.6	1.8	tr		3.4

1. Siphon Draw Member, average of 10 samples ±1 σ
2. Dogie Spring Member, average of 4 samples ±1 σ
3. Canyon Lake Member, average of 6 samples ±1 σ
4. Geronimo Head Fm - ash flows, average of 9 samples ±1 σ
5. Geronimo Head Fm - lavas, average of 4 samples ±1 σ
6. Apache Leap Fm from Haunted Canyon ±2 σ (Peterson, 1961, p. 130)
7. Apache Leap Fm, average of 3 samples from the type section ±1 σ
8. Apache Leap Fm, average of the Superior region data of Peterson (1961, p. 130).

Reproduced with permission of the copyright owner. Further reproduction prohibited without permission.

the plagioclase has a high temperature structural state, normal zoning (An_{40} to An_{26}), and common twin laws of Carlsbad, Carlsbad-albite and albite. Accessory minerals in the Superstition Tuff include sphene, zircon, apatite, augite and magnetite.

The Siphon Draw Member is the lowermost member of the Superstition Tuff and is the predominant unit in the southwestern portion of the area mapped. In Siphon Draw (plate 1) at the west end of the Superstition Mountains, the member overlaps the older dacite and attains its maximum thickness of 670 meters. At this locality nine separate ash flows may be distinguished. Each flow thins against the flanks of an older dacite dome and is separated above and below by a dacitic breccia and/or an airfall tuff (fig. 4). The breccias pinch out rapidly to the north and east, but contacts between flows may be traced around the main block of the Superstition Mountains as distinct color bands. Although these color bands are continuous for long distances, ash-flow units cannot be distinguished on the basis of chemistry, mineralogy or texture. Thus, where structure prevents tracing an ash flow contact back to Siphon Draw, the stratigraphic position of the flow could not be determined. However, because ash flow contacts represent originally horizontal planes, they could be used to interpret structures (such as faults) and strike and dip within the otherwise thick massive ash-flow sheet.

The second member of the Superstition Tuff is the Dogie Spring Member. It is exposed mainly along the eastern edge of the Superstition caldera (plate 1). The base of this member is not generally exposed, but the unit appears to be underlain and overlain by a rhyolite ash. In the region of Dogie Spring the unit is at least 200 meters thick. It is a simple cooling unit and appears to be made up of several flows as

Reproduced with permission of the copyright owner. Further reproduction prohibited without permission.

Figure 4 - Relationship of the Superstition Tuff to the older dacite complex as viewed in Siphon Draw.

Reproduced with permission of the copyright owner. Further reproduction prohibited without permission.

evidenced by partings and color bands parallel to the top of the sheet.

The uppermost member of the Superstition Tuff is the Canyon Lake Member. It is preserved mainly in a graben zone in the northern part of the area mapped. Near Tortilla Flat the tuff attains a thickness of 270 meters but the base is not exposed. At this locality the tuff is overlain by a rhyolite conglomerate. In the vicinity of the Willow Springs cauldron (west of the mapped area) the Canyon Lake Member rests on rhyolite ash flows and epiclastic breccias.

Chemical and normative data (table 2) confirm the classification of all three members of the Superstition Tuff as quartz latite (although by O'Conner's, 1965, classification they would be rhyolites). Although chemically similar the three members can be distinguished from one another by their modes (table 5). The Siphon Draw Member contains more quartz than plagioclase and more plagioclase than sanidine. The Dogie Spring Member contains more quartz than plagioclase and approximately equal amounts of plagioclase and sanidine. The Canyon Lake Member contains more plagioclase than quartz and approximately equal amounts of quartz and sanidine.

In outcrop the Superstition Tuff appears to be identical to the thick Apache Leap Tuff (Peterson, 1969). With one exception (8086), the chemical analyses of the two units are completely overlapping (table 6). However, the phenocrysts of the Apache Leap Tuff are nearly 75% plagioclase with quartz and sanidine comprising only about 10% and 3.4% respectively, by volume (table 5).

In order to confirm that the modal differences between the Superstition Tuff and Apache Leap Tuff are real and not a function of

Reproduced with permission of the copyright owner. Further reproduction prohibited without permission.

TABLE 6

AVERAGE CHEMICAL DATA FOR THE SUPERSTITION TUFF AND APACHE LEAP TUFF

	1	2	3	4	5
SiO_2	70.76	70.2	68.45	69.80 ±0.98	68.60 ±0.89
TiO_2	0.42	0.42	0.45	0.43 ±0.01	0.44 ±0.04
Al_2O_3	14.40	14.5	15.15	14.68 ±0.33	15.41 ±0.81
Fe_2O	2.25	1.8	2.2	2.08 ±0.20	2.32 ±0.40
FeO	0.46	0.52	0.42	0.47 ±0.04	0.36 ±0.31
MgO	0.68	0.65	0.76	0.70 ±0.05	0.70 ±0.22
MnO	0.07	0.07	0.07	0.07 ±0.0	0.08 ±0.01
CaO	1.79	1.08	2.15	1.91 ±0.17	2.24 ±0.23
Na_2O	3.66	3.9	3.30	3.62 ±0.25	3.93 ±0.18
K_2O	3.94	4.0	4.50	4.15 ±0.25	3.71 ±0.27
H_2O	1.28	1.93	2.05	1.75 ±0.34	1.99 ±0.80
P_2O_5	0.11	0.11	0.14	0.12 ±0.01	0.13 ±0.02

1. Siphon Draw Member, average of 3 analyses.
2. Dogie Spring Member, 1 analysis (AP-205).
3. Canyon Lake Member, average of 2 analyses (AP-234 & AP-235).
4. Average of 1, 2, and 3 $\pm$ 1 σ .
5. Apache Leap Tuff, average of 11 analyses $\pm 1\ \sigma$ (Peterson, 1961, p. 107-108).

Reproduced with permission of the copyright owner. Further reproduction prohibited without permission.

different point counting techniques, three samples from the type section of the Apache Leap Tuff were counted (table 5, # 7). The results indicate that the difference is real, and they point up a difference in counting technique. The difference is due to the size cut-off used in distinguishing phenocrysts from groundmass. The rocks contain many small plagioclase cleavage fragments which when counted increase the total phenocryst content and the percentage of plagioclase relative to the other phenocrysts.

Sample 8086 is not in good agreement with the other chemical analyses of the Canyon Lake Member, with which it is grouped on the basis of its mode. Although it appears to be fresh in thin section, the groundmass has undoubtedly been altered as indicated by the lack of ferrous iron. Further evidence for groundmass alteration is that sodium and calcium are low relative to the rest of the analyses of the Canyon Lake Member, while potassium is high. Lipman (1965) has demonstrated that this trend in volcanic rocks can be brought about by ground water leaching. Lipman and Van Alstine (1969) have further shown that this effect is due to ground water hydration of the glass (and not simply devitrification). Because sample 8086 is believed to be altered it is not used in the chemical average of the Canyon Lake Member (table 6) or in other chemical diagrams.

The Geronimo Head Formation

A rhyolite ash flow and epiclastic breccia sequence is interbedded with the Superstition Tuff. The basal ash flow unconformably overlies the Siphon Draw Member and the uppermost ash flow appears to be overlain by the Canyon Lake Member. Also interbedded with the Geronimo

Reproduced with permission of the copyright owner. Further reproduction prohibited without permission.

Head Formation are a series of silicic domes and lavas described in this report as "younger silicic domes and lavas", as well as some small mafic lavas.

The rhyolite ash flows and lahars attain a thickness of at least 430 meters and are best displayed at the type section, Geronimo Head (fig. 5). The formation is exposed throughout the northern two-thirds of the area mapped and is the predominant rock type in the Goldfield Mountains (Sheridan and Fodor, 1968). The base of the unit is marked by a partially welded to a nonwelded rhyolite ash flow which is overlain by interfingering epiclastic breccias and rhyolite ash flows.

In outcrop the rhyolite ash flows appear white, pale yellow and pinkish white. Lithic inclusions of dacite, Superstition Tuff and large blocks of pumice are common. Quartz, plagioclase, sanidine and biotite are all identifiable in hand specimen. The epiclastic breccias derived from these ash flows are similar in color and mineralogy to the above described rocks. The epiclastic breccias range from thinly bedded sandstones to thick lahars of boulders and fine ash (fig. 6).

In thin section the ash flows and lahars are quite similar except that ash flow textures (such as abundant tricuspate shards) are lacking in the lahars. The matrix of the lahars is more granular and often exhibits bedding. In both types of rock the matrix is largely devitrified ash which is altering to zeolites, probably clinoptilolite. Both rocks contain abundant pumice and lithic inclusions (up to 0.7 millimeters in diameter in the ash flows).

Although the ash flows and lahars have different phenocryst percentages, the relative abundances of minerals is nearly identical indicating that the lahars were derived directly from the ash flows

Reproduced with permission of the copyright owner. Further reproduction prohibited without permission.

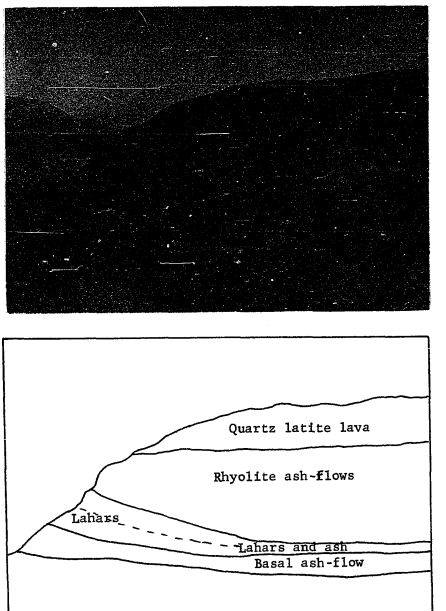

Figure 5 - View of Geronimo Head showing the relationship of the lahars and interfingering ash-flows.

Reproduced with permission of the copyright owner. Further reproduction prohibited without permission.

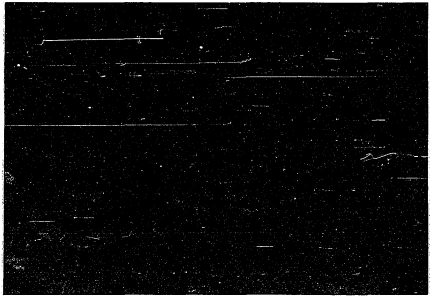

Figure 6 - View of typical lahar unit within the Geronimo Head Formation.

Reproduced with permission of the copyright owner. Further reproduction prohibited without permission.

(table 5). Quartz, which constitutes 36% of the phenocrysts, is clear and strongly resorbed. Sanidine, which accounts for 24% to 27% of the phenocrysts, is clear and euhedral with $2V_x$ varying between 0 and 10^o, and is often twinned according to Carlsbad and Baveno twin laws. Plagioclase, which comprises 28% of the phenocrysts, is often strongly fragmented and commonly twinned according to the Carlsbad, Carlsbad-albite, and albite laws. The plagioclase shows normal and oscillatory-normal zoning with an average composition of An_{25}. Biotite is the dominant mafic, comprising about 7% of the phenocrysts, and is often oxidized.

There is a greater variety of accessory minerals in the lahar units than in the ash flows. The ash-flow accessories are limited to sphene, hornblende, magnetite, zircon and occasional augite. The lahars contain the above with sphene, hornblende and augite becoming considerably more abundant. In addition, the lahars contain olivine and microcline. These are undoubtedly derived from older rocks.

The lack of a distinctive marker bed within the ash flow and lahar sequence and the presence of structural complexity prevents establishing a precise time sequence for the various ash flows. Even locating the uppermost or lowermost flows is a problem because a given flow may not have been deposited and/or preserved everywhere. For these reasons it is difficult to test the possibility of modal zoning in the rhyolite ash flows. The large standard deviation for the phenocryst percentage of a given mineral (table 5) is probably due to the low percentage of phenocrysts in the rock, but it may well indicate a change in the mode with time.

Two samples which appear to represent the base and top of the sequence (8103 and AP-215, respectively), indicate an increase in

Reproduced with permission of the copyright owner. Further reproduction prohibited without permission.

quartz and biotite and a decrease in plagioclase with time. Both samples were chemically analysed to check for chemical zonation (table 2) but both are too highly hydrated to be useful. Furthermore, both appear to have been affected by alkali transfer which has added potassium and removed sodium. The rock is classified on the basis of the normative and chemical data (table 2). Because this rock contains high silica and low alumina, and because nearly all the feldspar is alkali feldspar, the rock is classified as a rhyolite.

The Younger Mafic Lavas

Three small lenses of mafic lavas occur within the area mapped. They are informally referred to as the basalt of Willow Springs, the basanite of Black Mesa and the basalt of Canyon Lake. The oldest of these is presumed to be the basalt of Willow Springs. The basalt crops out as isolated buttes located within the Willow Springs cauldron. The tops of these buttes form a concordant surface which dips to the south-southwest.

The fresh rock is greyish-black and has only a limited exposure within the area mapped. It is more extensively exposed to the west where it is underlain and overlain by lahars of the Geronimo Head Formation.

The second oldest mafic lava is presumed to be the basanite of Black Mesa which caps both Black Mesa and Black Top Mesa (plate 1 and fig. 7). This unit has lahars above and below it and varies in thickness between 15 and 25 meters. Fresh surfaces are devoid of structures, with small red altered mafics set in a greyish-black groundmass. The weathered surface is generally knobby, but is locally affected by large scale spheroidal weathering.

Reproduced with permission of the copyright owner. Further reproduction prohibited without permission.

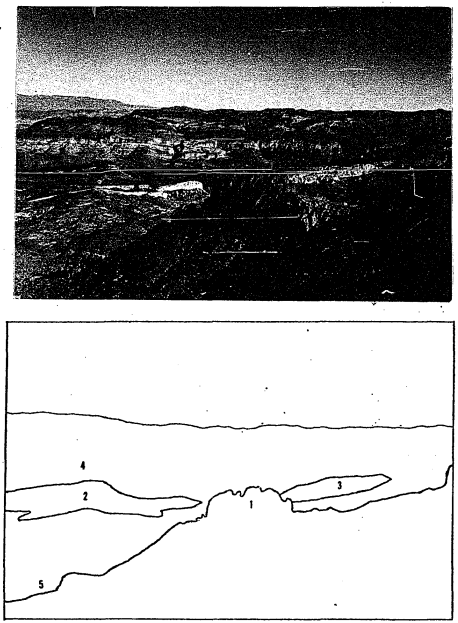

Figure 7 - View from the top of the Superstition Mountains (1) showing the concordancy of Black Mesa (2) and Black Top Mesa (3). The basal ash of the Geronimo Head Formation (yellow unit in 2 and 3) can be seen to thicken to the east, with unconformities above and below. The deep canyon between Geronimo Head (4) and Black Mesa (2) is fault controlled. A graben (5) lies between Black Mesa (2) and the Superstition Mountains.

Reproduced with permission of the copyright owner. Further reproduction prohibited without permission.

Two distinct flows can be mapped at Black Mesa (plate 1) and a third thin lens one or two meters thick is interbedded with the lahars above them. Three possible vents for the basanite can be located: a discontinuous dike south of Black Top Mesa; a small plug northeast of Black Mesa; and an area of vertical flow-banding in the center of Black Mesa. Ultramafic nodules which are often abundant in the vent areas of other Arizona mafic lavas are conspicuously absent at these possible vent areas and were not found anywhere in the flow.

The youngest of the mafic lavas is the basalt of Canyon Lake. This basalt crops out along the northern edge of Canyon Lake and is underlain by the Canyon Lake Member of the Superstition Tuff. The basalt is 10 to 15 meters thick and is vesicular at both the base and top. Olivine, now altered to iddingsite and red iron oxides, is concentrated just above the lower vesicular zone. The fresh rock is a medium light grey. Because the basalt thickens against a fault to the north and is not found on the south side of Canyon Lake, it must have flowed into a narrow north-dipping graben.

The three mafic lavas have distinctive modal and normative compositions (tables 2 and 3). The basalt of Canyon Lake is an alkali-olivine basalt with plagioclase as the dominant mineral in the whole rock. The plagioclase is normally zoned from An_{85} to An_{50}, averaging An_{67} based on maximum extinction angle normal to (010). These are most commonly twinned by the albite and Carlsbad-albite laws.

The basalt is coarsely trachytic to intergranular with olivine as the only phenocryst. Most of the olivine phenocrysts have altered to red iron oxides or iddingsite. Groundmass augite which constitutes about 17% of the whole rock is generally fresh showing hourglass zonation near extinction. Small grains of magnetite are common. Secondary calcite and

Reproduced with permission of the copyright owner. Further reproduction prohibited without permission.

zeolites, possibly natrolite on the basis of optical determinations, fill fractures and a few vesicles.

The basanite of Black Mesa is distinguished by the presence of anhedral nepheline crystals (16%) and nepheline in the groundmass. In some cases nepheline occurs as large poikolitic patches in a pilotaxitic to intergranular matrix. Subhedral to euhedral augite constitutes 62% of the phenocrysts and approximately an equal percentage of the groundmass. The augite is occasionally twinned on (100) and generally exhibits an hourglass extinction. Microprobe analysis indicates that the augite contains only about 3% Fe and 18% Mg by weight (Stuckless, 1969). These values are approximations arrived at by comparison with determination curves of Keil and Fredriksson (1964). Calcium was looked for qualitatively and found.

Augite is pale green in plane polarized light and is thus easily distinguished from the clear phenocrysts, but is generally lacking in the groundmass. Accessory minerals are limited to zeolite, possibly thompsonite on the basis of optical determinations, and magnetite which makes up about 15% of the groundmass. A few samples, particularly those collected near the vent areas, contain small cognate inclusions.

The modal analysis (table 3) demonstrates the remarkable uniformity of the basanite of Black Mesa and, combined with the normative mineralogy (table 2), provides the basis for classification. Wilkinson (1967, p. 167), defined basanite as a rock with more than 5% normative nepheline and with both modal nepheline and feldspar. The basanites are distinguished from other tephrites by the presence of olivine phenocrysts (Williams, and others, 1954, p. 59). The basanite of Black Mesa fits these restrictions. However, it is greatly enriched

Reproduced with permission of the copyright owner. Further reproduction prohibited without permission.

in aluminum and slightly enriched in calcium relative to the average nephelite basanite of Daly (1933, p. 23) and a nepheline basanite reported by Wilkinson (1967, p. 192). These latter basanites contain slightly more magnesium and total alkalies than the basanite of Black Mesa.

The basalt of Willow Springs is distinguished from the basalt of Canyon Lake by the presence of augite phenocrysts and from the basanite of Black Mesa by the lack of modal nepheline. The texture is generally intergranular to pilotaxitic with an estimated 20% of the groundmass composed of iron oxides. Augite accounts for approximately 70% of the phenocrysts and about 50% of the groundmass. Olivine is the only other signifcant phenocryst (30%) and is nearly absent in the groundmass. Plagioclase makes up an estimated 30% of the groundmass.

This lava is classified as an alkali-olivine basalt bordering on basanitoid. Wilkinson (1967, p. 167) defined alkali-olivine basalt as a rock with more than 5% modal olivine and less than 5% normative nepheline. From tables 2 and 3 it can be seen that the basalt of Willow Springs meets these criteria.

Younger Silicic Domes and Lavas

The ash--flow volcanism was accompanied and followed by the intrusion of quartz latite and rhyolite domes. In many places the intrusions broke through the surface producing lava flows which are interbedded with and unconformably overlie the Geronimo Head Formation. The lava flows are often only about 20 meters thick, but the quartz latite which caps Geronimo Head (fig. 5) attains a thickness of 170

Reproduced with permission of the copyright owner. Further reproduction prohibited without permission.

meters. The silicic domes have an arcuate distribution about the Black Mesa cauldron and the Superstition caldera (plate 1). The arc about the Superstition caldera appears as a semicircle within the area mapped, but a few quartz latite domes crop out south of the area mapped.

In the field the late lavas and domes may be distinguished from the older dacite complex by their glassy textures. In outcrop the rhyolites and quartz latites are most easily differentiated on the basis of phenocryst percentages. The rhyolites range from 7% to 4.5% phenocrysts which are plagioclase, biotite and hornblende with traces of quartz, sphene and augite (table 4). The quartz latites generally contain 23% to 38% phenocrysts which consist of plagioclase, hornblende, biotite, quartz and sanidine in order of decreasing abundance.

The rhyolites are almost always glassy domes with colors ranging from greyish-black to very dark grey or grey as the amount of hydration of the glass increases. These glassy rocks may show considerable devitrification, but in general the devitrification is limited to the formation of minor jasper spherulites.

When viewed in thin section the rhyolites exhibit abundant perlitic cracks through a glassy groundmass which encloses a few large euhedral to subhedral crystals of plagioclase, hornblende and biotite. The plagioclase exhibits normal zonation from An_{34} to An_{24} and is twinned according to the albite, Carlsbad-albite, and pericline laws. In some cases, the crystals occupy the centers of spherulites. Accessory minerals in the rhyolites are limited to magnetite, sphene, hematite, augite and possibly fayalite.

Reproduced with permission of the copyright owner. Further reproduction prohibited without permission.

The quartz latites are found as both domes and lavas. The former are flow-banded ranging in size from a few meters across to 700 meters at Apache Gap (fig. 8). The devitrified layers of flow-banded rocks show color alternation from greyish red to light pink. The lava flows exhibit crystals of plagioclase, hornblende, biotite and quartz (in order of decreasing abundance) set in a grey, glassy matrix.

The quartz latites are divided into two groups (table 4): those with phenocrystic quartz greater than 10% and those with phenocrystic quartz less than 10%. This division is arbitrary as the chemical data (table 2) show a continuous range throughout the quartz latite field. Both groups exhibit glomeroporphyritic phenocrysts set in a vitric to devitrified groundmass. The plagioclase is subhedral to euhedral and exhibits normal and oscillatory normal zoning (An_{32} to An_{25}). In some cases the plagioclase exhibits a wormy texture due to remelting (fig. 9). Both types contain euhedral oxyhornblende and biotite. Where present the quartz is usually deeply embayed and may exhibit undulatory extinction. Accessory minerals include euhedral sanidine, sphene and zircon. The sanidine is occasionally twinned according to the Baveno and Carlsbad laws.

The younger dome which crops out just north of Miners Needle is distinctively different from the rest of the domal rocks. The groundmass of AP-212 is granophyric and encloses embayed crystals of quartz, euhedral sanidine, anhedral plagioclase and biotite.

The classification is based on the normative mineralogy (table 2) with quartz greater than 10% and orthoclase greater than one-third, but less than two-thirds of the total feldspar. The chemical and normative data for samples 8011 and AP-27a are typical of the rhyolite

Reproduced with permission of the copyright owner. Further reproduction prohibited without permission.

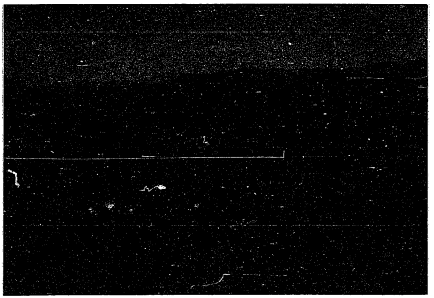

Figure 8 - Flow banded quartz latite lava. The lava flow originated at the ruptured wall of the dome (left edge of photo) and flowed to the northeast (right edge of photo.)

Reproduced with permission of the copyright owner. Further reproduction prohibited without permission.

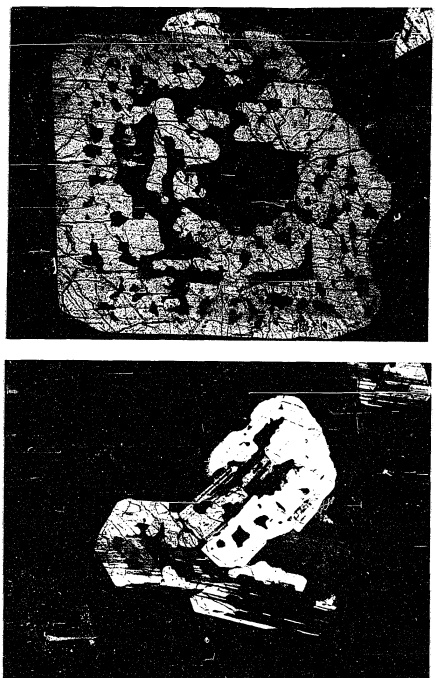

Figure 9 - Photomicrographs of remelted plagioclase phenocrysts in sample Ap-219. Both photographs taken at 35 X and with crossed nicols. The hole in the euhedral hornblende (lower photograph) is due to plucking during thin section preparation.

Reproduced with permission of the copyright owner. Further reproduction prohibited without permission.

class although by strict classification they are also quartz latites. Because they contain high silica and low alumina and because alkali feldspars constitute nearly all of the total feldspar, these rocks are classified as rhyolites.

Reproduced with permission of the copyright owner. Further reproduction prohibited without permission.

GEOCHRONOLOGY

The Precambrian Granitic Basement

The Precambrian rocks were dated by Rb-Sr isotope method. Plagioclase, potassium feldspar and biotite typically comprise 70% to 80% of these rocks and account for essentially all of the Rb and Sr. Because these minerals have greatly different Rb/Sr and $^{87}Sr/^{86}Sr$ ratios, the whole rock samples used were large (one to two kilograms) and were finely crushed (-100 mesh) before final splitting. It is believed that this procedure made sampling error small relative to other sources of error.

Samples of 1 to 0.5 grams were split off and dissolved in clean teflon or platinum crucibles. The dissolutions were accomplished using analytical grade HF, H_2SO_4 and HCl. The dissolution residues were evaporated and then leached with 2.6 N HCl and centrifuged. The HCl was made by bubbling HCl gas through triple distilled water. The Sr was separated from Rb in an ion exchange column with analytical grade Bio-rad AG-SOW-X8, 200-400 mesh resin. Blank measurements for Sr and Rb show Sr always less than 0.1 micrograms per analysis (Mark, personal communication, 1971). The spikes used were enriched in ^{84}Sr and ^{87}Rb and were added at the start of the dissolution.

All mass analyses were made on a 30 cm radius 90° sector, single focusing mass spectrometer using a triple filament ionization mode and a simple Faraday cage as the collector.

Reproduced with permission of the copyright owner. Further reproduction prohibited without permission.

The purified elements were loaded as chlorides on previously outgassed rhenium filaments. The isotopic composition of strontium was normalized to a Sr^{86}/Sr^{88} ratio of 0.1194. During this study a Sr^{87}/Sr^{86} value of 0.7083 $\pm$ 0.0001 was determined for the Eimer and Amend strontium standard.

The Sr^{87}/Sr^{86} values were calculated from the spiked analyses after correcting for machine discrimination. The precision of these measurements is estimated at $\pm$ 0.0004. The concentrations of Rb were calculated using raw machine ratios for the spiked samples and common Rb. The precision of these measurements is estimated at 1.5%. The results for the Rb and Sr isotopic measurements are reported in table 7. The errors reported are given in the 95% level of confidence.

The ages reported in table 7 are calculated according to the two-error regression of McIntyre and others (1966) by use of the U.S. Geological Survey program D0201. This program uses a Rb^{87} decay constant of 1.39×10^{-11} yr^{-1}. The data for the younger quartz monzonite fit an isochron within the limits of experimental error (model 1 of McIntyre and others, 1966). This age agrees closely with that determined by fission-track dating of sphene from the granite (1390 $\pm$ 40 m.y., table 8). Together, the two methods suggest that the younger quartz monzonite was emplaced approximately 1390 m.y. ago and has not been subjected to large thermal or chemical disturbances since its emplacement.

Damon (1968, p. 9), summarizes Rb-Sr whole rock and mineral isochron ages as being from 1450 to 1400 m.y. for "granitoid batholiths such as the Ruin granite of the Salt River Canyon, Gila County and Oracle

Reproduced with permission of the copyright owner. Further reproduction prohibited without permission.

TABLE 7

Rb-Sr ISOTOPE DATA AND AGES FOR THE GRANITIC BASEMENT OF THE SUPERSTITION AREA

Sample number*	Sample type	Calculate Sr^{87}/Sr^{86}_N	$Sr^{86} \times 10^{-8}$ moles/g	$Rb^{87} \times 10^{-8}$ moles/g	Rb^{87}/Sr^{86}
AP-202[a]	whole rock	0.80809	14.85	77.61	5.226
AP-202[a]	plagioclase	0.70714	55.73	7.120	0.1277
AP-202[a]	biotite	7.7679	0.9609	347.9	363.1
8145[a]	whole rock	1.0906	7.209	142.2	19.72
AP-209[b]	whole rock	0.73607	31.44	42.85	1.363
AP-211[b]	whole rock	0.72309	37.70	26.42	0.7010
AP-231[b]	whole rock	0.99187	7.461	97.90	13.12
8144[b]	whole rock	0.76691	22.64	61.99	2.738

* Sample locations are shown on plate 1 except 8144 and 8145 which were collected NW of the mapped area on Hwy 87 at the edge of the Adams Mesa quadrangle and 1000 feet north of Shea Boulevard, respectively.

a Calculated age by model #1 = 1395 ± 45 m.y.
$Sr^{87}/Sr^{86}_i = 0.70470 \pm .0017$

b Calculated age by model #3 = 1540 ± 84 m.y.
$Sr^{87}/Sr^{86}_i = 0.70738 \pm 0.00257$

Sr^{87}/Sr^{86}_N are normallized to $Sr^{86}/Sr^{88} = .1194$.

Reproduced with permission of the copyright owner. Further reproduction prohibited without permission.

TABLE 8

FISSION TRACK AGES FOR THE SUPERSTITION VOLCANIC SEQUENCE AND PRECAMBRIAN BASEMENT*

Sample number	Unit	Zircon (age in m.y.)		Sphene (age in m.y.)		Apatite (age in m.y.)
AP-244	quartz poor dacite	28.7 29.6 30.0 28.6 28.9 28.8	29.0± 0.5			
AP-236	Siphon Draw Member	24.9 24.3 24.1 25.4 23.9	24.5± 0.4	25.4 25.2 26.0 26.0 24.3 24.1 25.0 23.8 25.2 27.2 25.9 26.3	25.4± 0.9	
AP-232	Siphon Draw Member	24.7 24.8 24.2 22.6 23.6 25.3	24.2± 0.5	26.6 25.0 21.6 20.5 24.0 24.1 23.0 24.3 22.7 21.8 23.0 25.3 22.2	23.4± 0.9	24.8±2.3
AP-27a	Rhyolite dome	16.8 18.5 13.5 16.4 14.6 16.0	16.0 ± 1.3			

Reproduced with permission of the copyright owner. Further reproduction prohibited without permission.

TABLE 8--Continued

Sample number	Unit	Zircon (age in m.y.)		Sphene (age in m.y.)		Apatite	
AP-200	quartz latite lava	17.1 15.5 17.5 16.3 14.4 15.8	16.1± 0.8	11.2 17.0 16.5 16.3 20.1 13.5 17.5 16.5 16.0 14.8 16.5 15.8 17.8 16.2	16.1± 1.1		
AP-234	Canyon Lake Member	15.4 15.6 14.2 15.8 13.6	14.9± 0.8	15.7 14.7 15.8 16.3 15.5 13.5 14.3 17.7 15.5	15.4± 0.8		
AP-201	Ruin Granite			1440 1410 1380 1340	1393± 40	49.9 48.9 50.5 51.0	50.1± 0.8
AP-211	Madera Quartz Diorite			1304 1484 1484 1406 1305 1356	1390± 60		

*The ages following the brackets are averages $\pm 2\sigma$

Reproduced with permission of the copyright owner. Further reproduction prohibited without permission.

granite from the northern Santa Catalina Mountains in Pinal County." The age obtained for the younger quartz monzonite is in good agreement with this episode of plutonism.

The Sr isotope data for the older quartz monzonite do not fit an isochron within the limits of experimental error. The best fit is obtained with model 3 which is applicable for samples having different initial Sr^{87}/Sr^{86} ratios and systems which have not remained completely closed (McIntyre and others, 1966, p. 5464). Because the samples used exhibit minor alteration when viewed in thin section and because of their close proximity to the younger intrusion, the latter interpretation is preferred. The higher initial ratio for the older rocks is in accord with this interpretation, but may be due to an earlier high grade metamorphic origin as indicated by textures observed in outcrop.

The fission-track age determined for sphene from the older plutonic rock (1390 $\pm$ 60 m.y., table 8) also indicates that the older pluton has not remained a closed system since its formation. The fission-track date indicates that the rock was heated above 500°C at the time the granite was intruded (Naeser, personal communication, 1971). This heating could have been accompanied by an incomplete redistribution of Rb and/or Sr.

If the rocks of the older pluton have been disturbed, the measured Rb-Sr age will probably be too young. A major plutonic and orogenic episode is well documented in Arizona and adjacent areas between 1650 and 1760 m.y. (for summary see Livingston and Damon, 1968). Silver (1966) has obtained an U-Pb isotopic age on zircon of 1660 m.y. at Sunflower (north of the area mapped). By comparison with these dates

Reproduced with permission of the copyright owner. Further reproduction prohibited without permission.

the older quartz monzonite appears to yield an age which is too young. This result can be produced by a slight redistribution of Sr and Rb and is therefore in accord with experimental data. It is therefore concluded that the older quartz monzonite may be correlated with the Madera quartz diorite.

The Tertiary Volcanic Sequence

The Tertiary volcanics have been dated by use of fission tracks and K-Ar ratios. These data are reported in tables 8 and 9 respectively. The procedure used in the fission-track dating is essentially the same as described by Naeser and McKee (1970) except that the sphene mounts were etched in 50N NaOH at 130° to 150°C for 45 minutes. The "±" following a zircon or sphene age is two times standard error of the mean. The "±" for the apatite age represents one standard deviation and is calculated from the induced, fossil, and standard track densities.

Zircons from a quartz-poor dacite of the older dacite complex yield an age of 29.0 ± 0.6 m.y. This may well represent the oldest age of the older dacite complex as the sample dated was collected at the base of one of the largest domes. The uppermost flows of this unit intertongue with ash of the Siphon Draw Member of the Superstition Tuff (fig. 4), and therefore, the age of this tuff places an upper limit on the age of the older dacite complex. The average of the five mineral dates on this tuff is 24.4 ± 0.7 m.y. From these data it appears that dacite volcanism lasted at least five million years.

A comparison of the five fission-track ages for the Siphon Draw Member (table 8) with K-Ar ages (table 9) shows that only three of

Reproduced with permission of the copyright owner. Further reproduction prohibited without permission.

Reproduced with permission of the copyright owner. Further reproduction prohibited without permission.

TABLE 9

K-Ar DATA AND AGES FOR THE SUPERSTITION VOLCANIC SEQUENCE

Sample number	Unit	Type	K_2O %	$Ar^{40}Rad$ $x10^{-10}$ moles/g	Ar^{40}/K^{40} $x10^{-3}$	$Ar^{40}Rad$ %	Age m.y.
8074[a]	Siphon Draw Member	biotite	8.94	2.53 3.16 3.02 2.99	1.34	17.6 34.2 52.4	22.6±1.0
8073[a]	Quartz latite dome	biotite	8.93	2.91 2.78 2.82	1.26	21.2	21.3±1.0
8062[a]	basanite	whole rock	1.85	0.490	1.05	11.4	17.8±3.1
AP-205[b]	Dogie Spring Member	biotite	8.76	2.388	1.079	56.0	18.4±0.6
AP-215[b]	Geronimo Head ash flow	sanidine	8.50	2.050	0.9563	79.8	16.3±0.5
[c]	Apache Leap Tuff	biotite					19.9±0.9

a. From Damon, P. E., 1969, p. 49. Averages are weighted.
b. M. L. Silberman, written communication, 1970.
c. From Damon, P. E., and Bikerman, M., 1964, p. 72.

the dates overlap at the 1σ level of confidence, but that all overlap at the 2σ level. The agreement between the two methods can be improved slightly if the K-Ar age is recalculated by omitting the first Ar analysis. The resulting age of 23.5 $\pm$ 0.5 m.y. then agrees with the mean fission-track age of 24.4 $\pm$ 0.7 m.y.

The age of the lowermost ash flow in the Geronimo Head Formation can be bracketed. The basal ash flow and lahars overlie the Siphon Draw Member and are cut by a quartz latite dome which has been dated (sample 8073, table 9). This dome at Apache Gap bowed up the lahars on either side (fig. 10) and broke through to the surface flowing northward unconformably over the truncated lahar beds. The rhyolite volcanism must have commenced between 24.4 $\pm$ 0.7 and 21.3 $\pm$ 1.0 m.y. ago.

The last rhyolite ash flow has been dated at 16.3 $\pm$ 0.5 m.y. by K-Ar ratios in sanidine (table 9). This age is in agreement with two fission-track ages on the quartz latite lava which immediately overlies this ash flow (16.1 $\pm$ 1.0 m.y. and 16.1 $\pm$ 2.0 m.y. for zircon and sphene respectively, table 8) and with a fission-track age on a dome which cuts the Geronimo Head Formation (16.0 $\pm$ 1.6 for zircon, table 8). From these data it is concluded that the rhyolite volcanism lasted from eight to six million years.

During this interval several other volcanic rock types were erupted. The basanite of Black Mesa has been dated by K-Ar ratios in the whole rock at 17.8 $\pm$ 3.1 m.y. No date was obtained for the basalt of Willow Springs but it overlies Geronimo Head lahars and was deformed by the quartz latite intrusion at Apache Gap (fig. 10). Its age, therefore, is bracketed between 24 and 21 m.y. Most of the quartz latite domes and lavas must have erupted between 24.4 and

Reproduced with permission of the copyright owner. Further reproduction prohibited without permission.

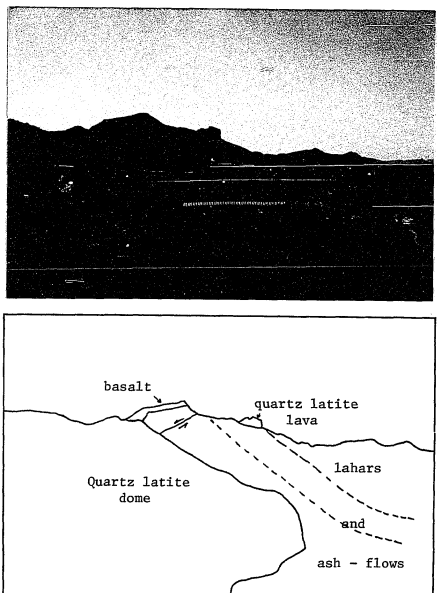

Figure 10 - Up doming of lahars and basalt by the intrusive dome at Apache Gap. A quartz latite lava, erupted from the dome, unconformably overlies the tilted lahar beds.

Reproduced with permission of the copyright owner. Further reproduction prohibited without permission.

16.1 m.y as none were found to underlie the Siphon Draw tuff and most either cross-cut or intertongue with the Geronimo Head Formation. There is some evidence to indicate that the fresh black glassy quartz latite and rhyolite domes formed after 16.1 m.y. Most of the rhyolites appear to cut the Geronimo Head Formation and the younger domes, and one dike north of Dogie Spring (plate 1, near sample AP-219) cuts the lava which is dated at 16.1 m.y.

The Dogie Spring Member is also interbedded with the Geronimo Head Formation and has been dated at 18.4 $\pm$ 0.6 m.y. (table 9). Although this age overlaps with the age of the Apache Leap tuff, it has been named as a separate unit on the basis of its modal data (table 5).

The youngest member of the Superstition Tuff is the Canyon Lake Member. Fission-track ages on this unit are 14.9 $\pm$ 0.9 m.y. for zircon and 15.4 $\pm$ 1.2 m.y. for sphene. These ages are in good agreement with the field relationships which suggest that this tuff is younger than the Geronimo Head Formation and most of the silicic domes and lavas. Because the basalt of Canyon Lake overlies this unit it must be younger than 15 m.y. The youngest unit exposed in the area is a flat-lying rhyolitic conglomerate which is less than 15 m.y. old.

Reproduced with permission of the copyright owner. Further reproduction prohibited without permission.

INITIAL SR^{87}/SR^{86} RATIOS AND THEIR IMPLICATIONS

Introduction

The use of Sr^{87}/Sr^{86} initial ratios to indicate the possible source areas for igneous rocks was proposed by Faure and Hurley (1963) and Hedge and Walthall (1963). The principles and assumptions of the model are simple. First, it is assumed that Sr isotopes do not fractionate geochemically. Evidence supporting this assumption is discussed by Doe and others (1966, p. 466-468). Secondly, it is assumed that the Rb^{87} decay constant is independent of temperature and pressure. There appears to be no evidence contrary to this assumption. Finally, it is assumed that at the time of the earth's formation the isotopic composition was homogeneous and that the Sr^{87}/Sr^{86} ratio was 0.6983 (Hedge and Walthall, 1963).

If these assumptions are accepted, then possible source areas may be characterized by their Sr^{87}/Sr^{86} ratios if they have different Rb/Sr ratios and if they have existed separately as closed systems for a sufficiently long period of time. Hedge (1966) reports the range in Rb/Sr values in the mantle as 0.01 to 0.05 with an average value of 0.025. This value yields a present day Sr^{87}/Sr^{86} range of 0.7045 to 0.7025 with an average value of 0.7040. He attributes the range in Rb/Sr ratios to regional inhomogeneities in the upper mantle. Doe (1968) characterizes Rb/Sr inhomogeneities in the mantle as being slightly higher under the oceanic ridges and under the continental interior.

Reproduced with permission of the copyright owner. Further reproduction prohibited without permission.

Doe (1968) suggests that the lower crust should be considered as a possible magma source area. If the lower crust is assumed to have an age of 2500 m.y. and an average Rb/Sr ratio of 0.05, then the resulting rocks would have Sr^{87}/Sr^{86} values of 0.704 to 0.706 (Doe, 1968, p. 155). Warren (1969) has reported the minimum thickness for this layer as five kilometers under the Superstition Mountains, and has reported the depth to the M-discontinuity as being 28 kilometers below sea level.

Analytical Procedure

Analyses on whole rock samples were performed on splits from one to two kilograms of sample. Approximately eighty grams were ground to -100 mesh and final splits of about one gram were then taken for isotope analysis and four gram splits were taken for X-ray fluorescence analysis. The mineral separates analysed were generally made on 60-100 mesh fractions and were accomplished using standard physical techniques. The samples were inspected under the microscope and cloudy feldspars were removed by hand picking. The cloudy feldspars were believed to represent xenocrystic material from the basement rocks which was not in isotopic equilibrium with the melt.

The samples were dissolved in clean platinum or teflon crucibles using analytical grade HF and either analytical grade $HClO_4$ or analytical grade H_2SO_4. The dissolution residues were evaporated to dryness, leached with triple distilled 2.6N HCl and then centrifuged. The Sr was separated on ion exchange columns containing 15 ml of analytical grade Bio-rad AG-50W-X8 200-400 mesh resin.

The Sr was analysed on a 30 cm radius 90° sector single focusing mass spectrometer. Ionization was accomplished with a triple filament

Reproduced with permission of the copyright owner. Further reproduction prohibited without permission.

mode and a simple Faraday cage was used as the collector. The $^{86}Sr/^{88}Sr$ ratio was assumed to be constant in nature with a value of 0.1194. All variance from this value was assumed to be due to machine discrimination and analyses on each sample were therefore normalized such that $^{86}Sr/^{88}Sr = 0.1194$.

Systematic drift in the machine was checked by periodic analyses of the Eimer and Amend reagent $SrCO_3$. Four analyses varied from 0.70824 to 0.70842 with no systematic variation. Ten analyses by R. Mark (personal communication, 1971) during the same period of time showed a similar range with no systematic variation.

Results reported are believed to be reproducible within 2 in the fourth placed based on four duplicate analyses. These yield an average reproducibility of $\pm$ 0.00018. Two mineral separates from the same stratigraphic horizon of the Siphon Draw Member and their corresponding whole rocks agree within 7 and 6 in the fifth place respectively (table 10). Rb and Sr concentrations were determined by X-ray fluorescence techniques which have a precision of $\pm$ 15%. The Rb/Sr ratios have a precision of $\pm$ 4% at the 95th level of confidence. Comparison of the values obtained by X-ray fluorescence (table 10) with those obtained by isotope dilution (table 7) and six duplicate analyses confirm this precision.

Results and Discussion

Noble and Hedge (1969) have suggested that devitrified volcanic rocks may not have the same apparent whole rock and phenocryst $^{87}Sr/^{86}Sr$ initial ratios. They attribute this disequilibrium to the action of groundwater. Thirteen mineral and whole rock pairs from the Superstition area were analysed. Of these, six pairs agreed within

Reproduced with permission of the copyright owner. Further reproduction prohibited without permission.

Reproduced with permission of the copyright owner. Further reproduction prohibited without permission.

TABLE 10

Rb AND Sr DATA ON WHOLE ROCK AND PHENOCRYST SEPARATES FROM THE SUPERSTITION VOLCANIC ROCKS AND PRECAMBRIAN GRANITIC BASEMENT

Sample number	Unit	Age m.y.	Sample type[1]	Sr^{87}/Sr^{86}_N	Sr^{87}/Sr^{86}_i	Rb* (ppm)	Sr* (ppm)	Rb/Sr*
AP-27a	Glassy rhyolite dome	10(?)	P	0.7055		6.0	1455	0.004
AP-213	Glassy quartz latite domes	15(?)	P	0.7057		3.6	1398	0.003
			Wr	0.7056	0.7055	85.9	609	0.141
AP-219			P	0.7107				
			Wr	0.7135	0.7131	289	416	0.716
AP-217	Devitrified quartz latite domes	15(?)	P	0.7073		21.1	639	0.033
			Wr	0.7082	0.7077	187	252	0.742
AP-212			Wr	0.7092	0.7089	145	322	0.450
AP-200	Devitrified quartz latite lava	16.1	P	0.7074		3.5	747	0.005
			Wr			133	414	0.321
8102	Black Mesa basanite #1	17.0	Wr	0.7062		14.7	1667	0.009
8110			Wr	0.7061		5.7	1857	0.003
8146			Wr	0.7064		14.9	1614	0.009
8111	Black Mesa basanite #2	17.0	Wr	0.7058		25.7	1423	0.018
8147			Wr	0.7059		18.6	1139	0.016
AP-215	Geronimo Head ash flow	16.3	P	0.7138	0.7136	16.5	58.6	0.281
			Wr			205	55.1	3.721
AP-240		23(?)	P	0.7139	0.7137			
			Wr			209	68.3	3.054

Reproduced with permission of the copyright owner. Further reproduction prohibited without permission.

TABLE 10--Continued

Sample number	Unit	Age m.y.	Sample type[1]	Sr^{87}/Sr^{86}_N	Sr^{87}/Sr^{86}_i	Rb* (ppm)	Sr* (ppm)	Rb/Sr*
	Superstition Tuff [2]							
AP-234	Canyon Lake Member	15.0	P	0.7080		5.7	995	0.006
	top		Wr	0.7090	0.7087	159	338	0.470
AP-235	middle		P	0.7094		2.1	1143	0.002
			Wr	0.7096	0.7093	188	343	0.548
AP-207	Dogie Spring Member	18.4	P	0.7062				
	top		Wr	0.7073	0.7071	93.1	380	0.245
AP-205	middle		S	0.7073	0.7071	119	548	0.217
			Wr	0.7078	0.7075	138	329	0.419
AP-208	base		P	0.7075		7.3	711	0.010
			Wr	0.7089	0.7082	138	136	1.012
AP-236	Siphon Draw Member	24.4	P	0.7064		6.3	741	0.009
	top		Wr	0.7076	0.7072	126	325	0.388
AP-245	base		P	0.7071		4.6	750	0.006
			Wr	0.7075	0.7071	123	333	0.368
AP-232	base		P	0.7072		3.0	828	0.004
			Wr	0.7075	0.7072	131	357	0.367
AP-244	Older dacite	29.0	P	0.7057		1.3	1728	0.001
	complex		Wr	0.7058	0.7057	56.5	763	0.074
AP-243	Older basalt	30(?)	Wr	0.7056		18.7	792	0.024
AP-201	Ruin Granite	1395	Wr	0.8939				
AP-202			Wr	0.8081		270	149	1.812
8145			Wr	1.0906		481	72.3	6.652

TABLE 10--Continued

Sample number	Unit	Age m.y.	Sample type[1]	Sr^{87}/Sr^{86}_N	Sr^{87}/Sr^{86}_i	Rb* (ppm)	Sr* (ppm)	Rb/Sr*
AP-209	Madera quartz diorite (altered)	1640	Wr	0.7361		146	287	0.509
AP-211			Wr	0.7231		71.3	309	0.231
AP-231			Wr	0.9919		370	77.7	4.762
8144			Wr	0.7669		193	203	0.949
AP-230			Wr	0.7343				

* - X-ray fluorescence analyses by Willis P. Doering.

1 - P = plagioclase, Wr = whole rock, and S = sanidine.

2 - Samples from the various members of the Superstition Tuff are subdivided by their stratigraphic position within each member.

Reproduced with permission of the copyright owner. Further reproduction prohibited without permission.

the limits of analytical uncertainty, but seven pairs had significantly higher Sr^{87}/Sr^{86} ratios in the whole rock.

If it is assumed that the Precambrian basement is the only possible source for the more radiogenic strontium, then three possible mechanisms can be proposed to explain the higher whole rock ratios: 1) The whole rock values may reflect lithic inclusions which were eliminated from the phenocryst fraction; 2) the devitrified glass may have exchanged Sr with ground water which obtained its strontium from the Precambrian basement; and 3) the melt may have assimilated radiogenic strontium faster than the phenocrysts could re-equilibrate isotopically.

Lithic inclusions were observed throughout the Superstition Tuff, but none were noted in the specimens analysed. Samples AP-217 and AP-219, which show large differences between phenocryst and whole rock ratios, are late stage domes which are apparently devoid of lithic inclusions. It is therefore concluded that lithic inclusions are not the cause of the higher Sr^{87}/Sr^{86} ratios in the whole rock samples.

Noble and Hedge (1969) report that devitrified rock may acquire as much as 20 ppm strontium during devitrification from ground water. If all of the additional strontium had the isotopic composition of the basement rock, the effect of ground water on the devitrified rock would be sufficient to explain the higher Sr^{87}/Sr^{86} ratios in the six devitrified whole rocks. Furthermore, ground water would not be expected to affect each specimen to the same degree, which is in agreement with the results.

Dasch (1969) reports the Sr^{87}/Sr^{86} ratio for phenocrystic plagioclase in a basalt as being 0.702 while the groundmass plagioclase

Reproduced with permission of the copyright owner. Further reproduction prohibited without permission.

Sr^{87}/Sr^{86} ratio is 0.704. This may be interpreted as isotopic disequilibrium between crystals and melt. Moorbath and Bell (1965) report a similar disequilibrium between xenocrysts and melt in the high level intrusions at Skye. In this case the xenocrysts retained their more radiogenic strontium. A disequilibrium causing the melt to be more radiogenic than the phenocrysts could occur if assimilation of radiogenic strontium were rapid relative to the rate of isotopic equilibration between liquid and crystalline phases.

This mechanism is the best one for explaining the higher whole rock Sr^{87}/Sr^{86} ratio in sample AP-219 because this rock is free of inclusions and is not devitrified. Furthermore, many of the minerals in it were partly remelted (fig. 9). Since this rock is very close in chemical composition to the Precambrian basement, it is reasonable to assume that quartz latite could melt and assimilate some basement rock when it began to remelt. Calculations based on the basement strontium composition and concentration show that the melt would have to assimilate less than 2% more crustal strontium than was assimilated by the phenocrysts.

It therefore appears that the strontium isotopic composition of the phenocrysts is the best indicator of the magma source region. A comparison of these data with the Sr^{87}/Sr^{66} ratios for the Precambrian basement (table 10) shows that the volcanics were not derived by a simple melting or partial melting of the granitic basement rocks. Seismic data suggest that granitic rocks extend about 22 km below sea level in the Superstition region (Warren, 1969). If the ages and Rb/Sr ratios of the granitic rock at the surface are representative of the granitic crust at depth, then the volcanic rocks must have been derived at depths in excess of 22 km.

Reproduced with permission of the copyright owner. Further reproduction prohibited without permission.

The lowest Sr^{87}/Sr^{86} ratios observed in the Superstition area are in the range of 0.7055 to 0.7057. These include the early basalt, older dacite, a late quartz latite dome and a late rhyolite dome. These ratios are high when compared with accepted mantle values in oceanic regions (i.e., less than 0.704). However, ratios in the range of 0.705 to 0.706 have been reported for apparently uncontaminated continental basalts of the western United States (Doe and others, 1969b; Pushkar, 1970). Doe and others, (1969a) report a Sr^{87}/Sr^{86} range of 0.7053 to 0.7056 for the basalt-rhyolite sequence of the Summer Coon volcanics of Colorado. Similar initial ratios have been reported for other mafic-silicic associations in Scotland (Summerhayes, 1966; and Moorbath and Bell, 1965) and New Zealand (Ewart and Stipp, 1968).

The large number of continental igneous rocks with initial Sr^{87}/Sr^{86} ratios in the range of 0.705 to 0.706 indicate a source region with this range in values. Furthermore, the rocks having these ratios exhibit a wide range of strontium concentrations. It would seem too fortuitous that each should assimilate only enough radiogenic strontium to raise its apparent initial ratio from less than 0.704 to 0.7055.

If the source which is producing 0.7055 initial ratios is 4.5 billion years old and had an original Sr^{87}/Sr^{86} ratio of 0.6983, then that source would need to have a Rb/Sr ratio of 0.035. Doe (1968) pointed out that such a mantle would give rise to a higher heat flow than that observed. If the lower crust separated from the mantle at 2.5 to 2.7 billion years ago and if its average Rb/Sr ratio is about 0.05, then it would currently have a Sr^{87}/Sr^{86} ratio of 0.7050 to 0.7055. Rocks

Reproduced with permission of the copyright owner. Further reproduction prohibited without permission.

in the compositional range of high silica basalt to andesite could have a Rb/Sr ratio of 0.05 (Hedge, 1966). This compositional range seems reasonable for the lower crust, and it is therefore concluded that the volcanic rocks were derived in the lower crust by either partial melting or complete melting and differentiation.

If the above arguments and assumptions are accepted, then it seems reasonable that very minor inhomogeneities in Rb and Sr could give rise to uncontaminated magmas with initial Sr^{87}/Sr^{86} ratios as high as 0.706. The larger variations in Sr^{87}/Sr^{86} could be explained by large Rb/Sr variations in the source region (0.05 to 0.10). Alternatively, the volcanic rocks could have been contaminated by the granitic crust during their ascent to the surface. Quantitative calculations based on the strontium concentrations and isotopic compositions of the volcanic and basement rocks show that less than 5% contamination is required to raise any of the volcanic rocks from 0.7055 to their observed initial ratio.

The strontium isotope data for the ash flows of the Superstition Tuff suggest that the magma was contaminated during its ascent. The base of each member is enriched in Sr^{87} relative to the top of the same member (table 10). These data are consistent with the model proposed by Noble and Hedge (1969) in which the upper portion of the magma incorporates crustal material during the ascent. This model is also consistent with Sr^{87}/Sr^{86} zoning in plutonic rocks (Hamilton, 1963, and Parkhurst, 1969).

Each member of the Superstition Tuff is enriched in Sr^{87} relative to the preceding member. This trend of increasing Sr^{87}/Sr^{86} with time is generally true of the entire volcanic sequence with the exception of two of the youngest domes (AP-219 and AP-27a) and the basanites.

Reproduced with permission of the copyright owner. Further reproduction prohibited without permission.

The latter contain so much strontium that they can mask relatively small amounts of crustal contamination. Furthermore, there is no suggestion either chemically or petrographically that these rocks have been contaminated. The late stage domes must represent late pulses from the source area which either erupted too quickly or at too low a temperature to allow contamination.

Reproduced with permission of the copyright owner. Further reproduction prohibited without permission.

OXYGEN ISOTOPE DATA

Oxygen isotope ratios were determined for each of the ash-flow tuffs in an attempt to determine the temperatures of crystallization. The results are presented in tables 11 and 12. The O^{18}/O^{16} fractionation between co-existing mineral phases crystallizing at equilibrium decreases with increasing temperature. In all known cases a linear relationship exists between the fractionation among co-existing phases and $1/T^2$, where temperature is in ^{o}K (Taylor, 1968, p. 2).

If a single mineral pair is used to determine the temperature of crystallization, equilibrium must be assumed. If more than one mineral pair is used, the degree of concordance of the resulting temperatures may be used to make inferences concerning equilibrium.

The normal range in δO^{18} contents of various magmas is known. Observed deviations from these values may be explained in terms of possible contaminating sources. Silicic volcanics have a normal δO^{18} range of 5.5 to 10.2 (Taylor, 1968) with modes between 7.0 and 8.3 for rhyolite through dacite lava flows and between 8.4 and 10.2 for rhyolite ash flows. The δO^{18} values for meteoric waters are generally negative with values in the southwestern United States of -3 to -7 (Craig, 1961). Thus, incorporation of meteoric water by the melt will tend to lower its δO^{18} value. Taylor and Epstein (1968) and Shieh and Taylor (1969) have shown that meteoric water has been incorporated by several shallow intrusive rocks especially along the

Reproduced with permission of the copyright owner. Further reproduction prohibited without permission.

TABLE 11

OXYGEN ISOTOPE MEASUREMENTS[a]

Sample number	Plagioclase	Biotite	Quartz	Sanidine	Magnetite
AP-205	8.05±0.03	7.47±0.18	9.56±0.10	8.98	
AP-213	8.82				
AP-215	9.12±0.02	7.24±0.15			
AP-219	8.90±0.18				
AP-234	8.35±0.10	7.84±0.05	9.70±0.24	9.06	4.76
AP-236	7.96±0.15	9.44±0.10	9.50±0.24		
AP-240	8.42±0.22				
T-111[b]	8.7	5.8 ±0.3	9.8		3.6±0.0

a. Values given as δO^{18} in parts per mil relative to SMOW. Analyses by J. R. O'Neil.

b. From Taylor (1968). Sample collected south side of Salt River, west of Horse Mesa Dam in a glassy rhyolite dome.

Reproduced with permission of the copyright owner. Further reproduction prohibited without permission.

TABLE 12

OXYGEN ISOTOPE TEMPERATURE DETERMINATIONS[a]

Sample[b] number	ΔQ-M	T_{Q-m}	ΔQ-B	T_{Q-B}	ΔP-M	T_{Q-M}	ΔP-B	T_{P-B}
T-111	6.2	805	4.0	745	5.1	750	2.9	750
LP-11	4.8	1040	2.3	1305	3.5	990	1.0	990
SCB-4	7.6	665	3.3	895	6.5	615	2.2	615
SCB-5	7.5	670	5.1	595	6.5	610	4.1	610
SCB-6	7.7	665	4.5	670	6.0	650	2.8	650
SRO-18							3.7	515
SRO-15A							4.2	545
HES-8					7.3	550	4.5	500
HES-4a					6.7	610	4.1	610
AP-215							1.9	850± 130
AP-234	4.94	1008±10	1.86		3.59	978±20	0.51	
AP-205			2.09				0.58	
AP-236			2.06				0.54	

a. Δ values in parts per mil. Temperatures in degrees centigrade, error estimate based on fractionation curve uncertainty ±1 σ not experimental error.

b. Sources of data: T-111, LP-11, SCB-4, SCB-5, and SCB-6, Taylor (1968); SCB-4, SCB-5, and SCB-6, Taylor and Epstein (1962); SRO-18, SRO-15A, and HES-4a, Shieh and Taylor (1969).

Reproduced with permission of the copyright owner. Further reproduction prohibited without permission.

margins and upper borders of the intrusions.

Taylor (1968) has shown that hydrated and devitrified glasses do not retain their original δO^{18} values. The measured values usually indicate an O^{18} exchange with meteoric waters at low temperatures. In such rock, however, the δO^{18} value in plagioclase phenocrysts may be taken as indicative of the δO^{18} value of the melt.

The δO^{18} values for the volcanic rocks analysed all fall in the normal range for silicic volcanic rock. The minor variations between the petrologic types can be explained by normal fractionation processes. In the most silicic rocks plagioclase tends to be depleted in O^{18} by 0.2 to 0.4 per mil relative to the melt (Taylor, 1968). The data for the domes, lavas and quartz latite ash flows are in good agreement with the predicted trend (fig. 11) and therefore suggest that they are genetically related. The two analyses of the rhyolite ash flows do not fall on this trend, but appear to fall on a parallel trend which is enriched in O^{18}. This suggests a slightly different genesis for the rhyolite ash flows. As already noted, the rhyolite ash flows are greatly enriched in Sr^{87} relative to the domes, lavas and quartz latite ash flows.

The data indicate that meteoric water was not incorporated during crystallization. However, two rhyolitic domes in the area have undergone extensive oxygen and hydrogen exchange with meteoric water at low temperatures during hydration (Taylor, 1968). This exchange has not affected the oxygen isotope ratios in the phenocrysts. A similar disequilibrium between phenocrysts and whole rock has been noted in the strontium isotopes. The oxygen isotope data support the conclusion that the strontium isotope disequilibrium may be due in part to the action of ground water.

Reproduced with permission of the copyright owner. Further reproduction prohibited without permission.

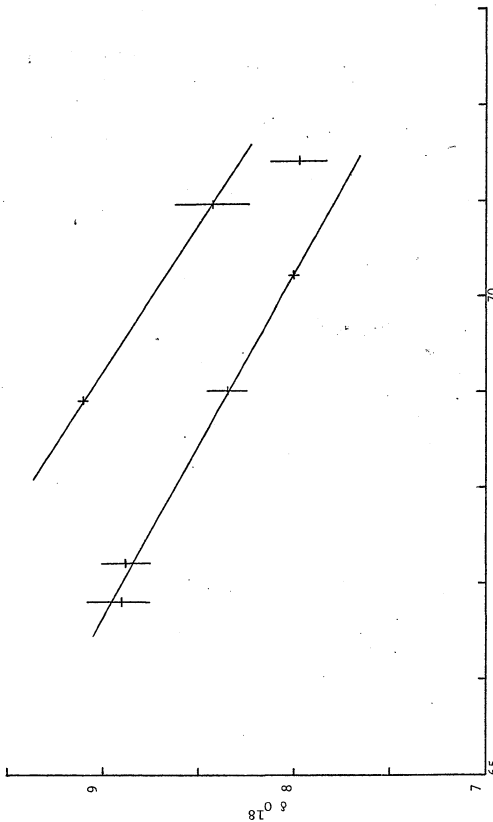

Figure 11 - The variation of δO^{18} in plagioclase phenocrysts as a function of the weight percent silica in the whole rock. The two samples in the upper trend are from the Geronimo Head Formation.

Reproduced with permission of the copyright owner. Further reproduction prohibited without permission.

Temperatures were determined by constructing fractionation curves based on a least squares refinement of published temperatures and fractionations (fig. 12). The data used and the resulting temperatures are given in table 12. The best known geothermometer is the quartz-magnetite which has been experimentally determined in the range of 250° to 800° C (O'Neill and Clayton, 1964). Both minerals have fairly constant chemical compositions, but they occur as secondary minerals in the Superstition volcanics and the quartz is generally resorbed, indicating a chemical disequilibrium. For these reasons an attempt was made to construct a feldspar-biotite geothermometer.

Such a thermometer will of necessity be inaccurate as it will be dependent on the chemical composition of both members. The δO^{18} value for plagioclases is known to vary with composition. For this reason, only plagioclases in the range of An_{20} to An_{40} were used in the calibration and the temperature used was from the plagioclase-magnetite determinations. The effects of Fe-Mg solid solutions and oxidation state of the biotite cannot be eliminated. For this reason there is considerable scatter in the fractionation curve (fig. 12c) which results in a large uncertainty in the temperature determinations.

The plagioclase-biotite fractionation in the three members of the Superstition Tuff is remarkably constant despite the fact that the δO^{18} value for each mineral varies from member to member. The fractionation of 0.55 results in a temperature of crystallization of 1140 $\pm$ 125°C. Experimental studies show that this is well outside the stability field for the coexistence of biotite, quartz and two feldspars.

The equilibrium assemblage of orthoclase, quartz, phlogopite, and liquid may exist in a water saturated magma along a P-T curve which passes through points at 825°C, o.5 kb total pressure and 750°C, kb total

Reproduced with permission of the copyright owner. Further reproduction prohibited without permission.

Reproduced with permission of the copyright owner. Further reproduction prohibited without permission.

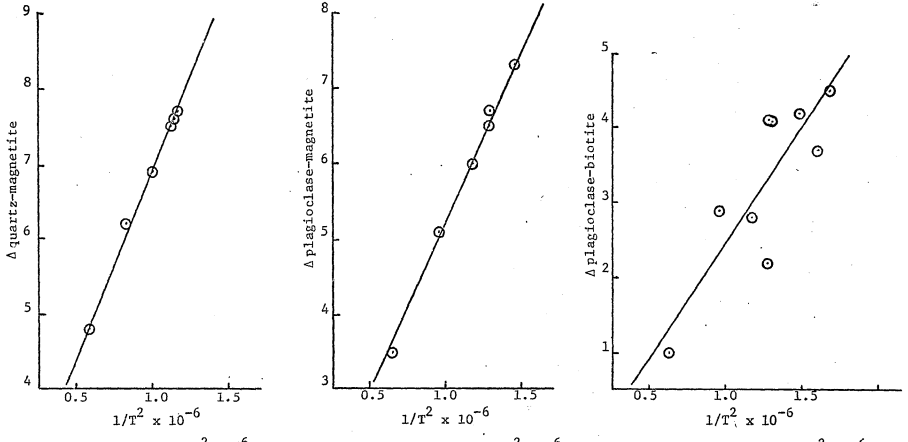

a) $\Delta Q - M = 5.07(1/T^2 x 10^{-6}) + 1.85 \pm 0.04$ b) $\Delta P\text{-}M = 4.56(1/T^2 x 10^{-6}) + 0.68 \pm 0.09$ c) $\Delta P\text{-}B = 2.91(1/T^2 x 10^{-6}) - 0.40 \pm 0.62$

Figure 12 - Oxygen isotope fractionation curves for quartz-magnetite, plagioclase-magnetite, and plagioclase-biotite. Data and data sources are listed in table 12.

pressure (Luth, 1967). Annite and two feldspars may co-exist on the QFM buffer at 600°C, 0.5 kb total pressure and 650°C, 4.0 kb total pressure. Substitution of Na for K in the annite structure reduces the maximum temperature for stable co-existence of these phases (Rutherford, 1969). These two experimental studies bracket the biotite composition in the Superstition Tuff (table 13).

Even if the magmas are assumed to be nearly anhydrous and if titanium is assumed to increase the stability of biotite, the maximum temperature of formation of biotite cannot be above 850°C and is probably much lower (perhaps 750°C). The inconsistency between experimental results and observed data is best explained by non-equilibrium crystallization. Both Luth (1967) and Rutherford (1969) found that biotite readily crystallized during the relatively rapid laboratory quench.

Temperatures determined by quartz-magnetite and plagioclase-magnetite fractionations in sample AP-234 (Canyon Lake Member) are consistent with one another and probably indicate that these three minerals were crystallizing in equilibrium at about 990° $\pm$ 20°C (table 12). If this temperature of first crystallization is accepted, then the biotite may well have formed in the quench. This quench was slow enough to allow the quartz to undergo a large amount of resorption and it is therefore likely that there was sufficient time to form large biotites.

The constancy of the plagioclase-biotite fractionation indicates that each of the three members of the Superstition Tuff underwent similar histories. It is therefore likely that all three members started crystallizing near 990°C. The plagioclase-biotite fractionation

Reproduced with permission of the copyright owner. Further reproduction prohibited without permission.

TABLE 13

PARTIAL CHEMICAL ANALYSES OF MINERALS

Sample number	Na_2O[a]	K_2O[a]	Mg[b]	Fe[b]	TiO_2[b]
AP-205					
biotite	0.6	8.76	7.8	11.9	4.0
sanidine	3.8	10.81			
AP-215					
sanidine	4.7	8.50			

a. Flame photometer analysis by C. O. Ingamells. Results in weight percent.

b. Microprobe analysis of L. Calk, average of 3 crystals. Results in atom percent for Fe and Mg. TiO_2 is estimated.

Reproduced with permission of the copyright owner. Further reproduction prohibited without permission.

in the rhyolite ash-flow tuff indicates a temperature of about $845^{\circ} \pm 130^{\circ}C$. This temperature is a little high when compared with experimental results (Luth, 1967 and Rutherford, 1969), but it could represent equilibrium crystallization, especially if the large error is considered. The lack of densely welded rhyolite ash flows in the Superstition region suggests that the rhyolites were not as hot as the quartz latites at time of eruption. Even if this fractionation is again the result of disequilibrium crystallization, it is significantly different from that obtained for the quartz latite ash flows and therefore consistent with a differing petrogenesis for the two types of ash-flow tuffs.

Four mineral pair temperatures were determined for a rhyolite dome southeast of Horse Mesa Dam (Taylor, 1967). Preliminary field relationships indicate that this dome is part of the same dome complex as sample AP-219. The temperatures measured are between 745° and $800^{\circ}C$ (table 12). This temperature range is in agreement with that determined for the rhyolite ash flows.

Reproduced with permission of the copyright owner. Further reproduction prohibited without permission.

ORIGIN OF THE MAGMAS

The study of the volcanic sequence in the Superstition Wilderness Area raises several major questions: 1) Do the results of the study of this volcanic area have any general applicability? 2) Are all the volcanics the product of a single differentiating magma chamber?; 3) If so, what was the parent material? 4) Why are rocks containing between 49% and 59% SiO_2 absent?; and 5) Why do the modal amounts of quartz-plagioclase-sanidine vary among the different quartz latite ash flows whereas the chemical compositions remain relatively constant?

As mentioned earlier, the general sequence of volcanic rocks throughout Arizona is basalt, andesite, quartz latite, rhyolite and basalt. Lipman and others (1970) have concluded that this sequence is typical of much of the Cenozoic volcanism in the western United States. These authors also point out that where the stratigraphy is accurately known through age-dating, the sequence starts with a lava and autoclastic breccia episode which gradually changes to an equally voluminous pyroclastic episode which is followed by a relatively minor basalt and rhyolite lava episode. Thus, because of its similarity to the pattern of Cenozoic volcanism in the western United States, conclusions drawn about the petrogenesis of the Superstition volcanics may well be generally applicable.

When the chemical data are recalculated as water-free and plotted on a silica variation diagram (fig. 13) an approximate Peacock index

Reproduced with permission of the copyright owner. Further reproduction prohibited without permission.

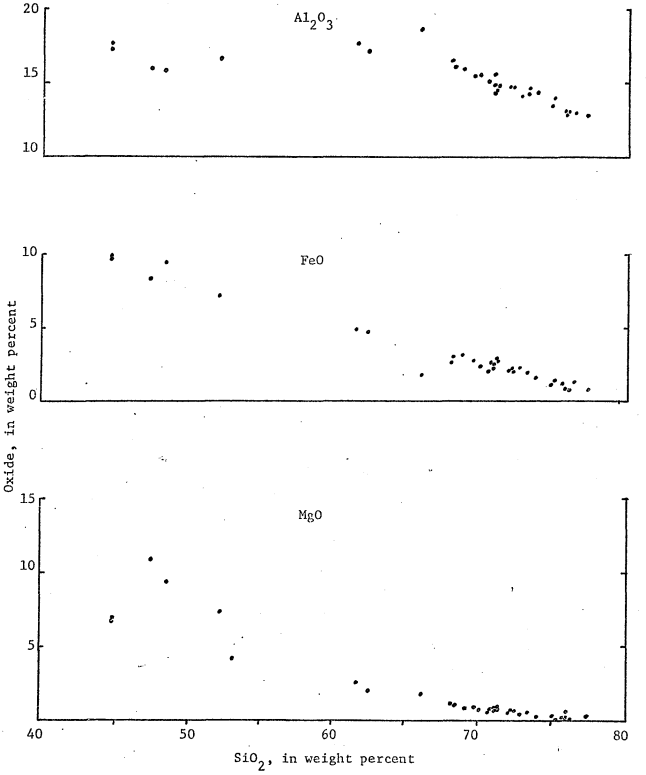

Figure 13 - SiO_2 - variation diagrams for weight percent of major oxides of the Goldfield and Superstition volcanics, calculated water-free. Data are from table 2 and Fodor, 1968.

Reproduced with permission of the copyright owner. Further reproduction prohibited without permission.

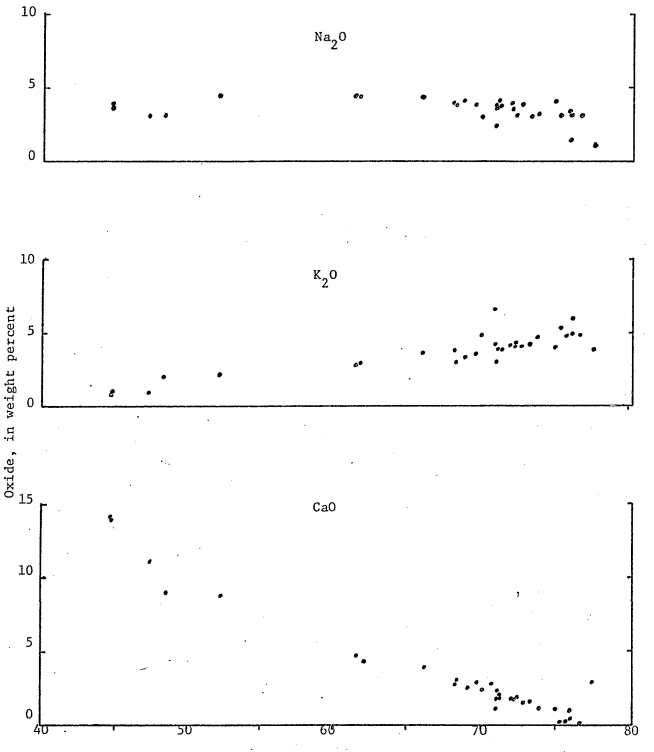

Figure 13 - continued.

Reproduced with permission of the copyright owner. Further reproduction prohibited without permission.

can be determined by projecting the lines of liquid descent through the region where no chemical analyses exist. The resulting intermediate index (54-56) is normally associated with non-orogenic environments (Barth, 1962). A further argument for a non-orogenic derivation can be made from the trend on an AMF diagram (Stuckless, 1969, p. 48-51). The normal non-orogenic trend shows an early enrichment in iron followed by a late stage enrichment in alkalies. The trend for the Superstition volcanics also shows an early enrichment in iron followed by a late enrichment in alkalies, although this trend is not as pronounced as that observed in some of the classic non-orogenic sequences. Thus, it may be that the processes acting in the Superstition region are typical of other non-orogenic igneous suites.

The data plotted on the silica variation diagram (fig. 13) show considerable scatter. This may be explained by the fact that a smooth trend represents the line of liquid descent. The data plotted on figure 13 are from porphyritic rocks. These data may not represent possible liquid compositions if there has been a relative movement between different species of phenocrysts (Bowen, 1928, p. 93). In some cases the deviation from the liquid lines of descent may be attributed to secondary alteration. Finally, some variation may be due to gas transfer of alkalies during differentiation. However, even with these limitations the diagram displays some useful information.

First, the silica variation diagram emphasizes the bimodal silica distribution. Secondly, it shows that the silicic rocks fit rather smooth trends indicating that all of these rocks could have developed from quartz-poor dacites by simple differentiation processes such as fractional crystallization. By this mechanism the early-formed

Reproduced with permission of the copyright owner. Further reproduction prohibited without permission.

plagioclase and hornblende would be removed from the melt. Thirdly, it shows that the basalts and basanites can be related to one another by fractional crystallization of a basaltic parent magma under different sets of physical conditions.

If the basalt containing 47.2% SiO_2 (sample 8026 recalculated) is taken as a starting point, then the basalts containing more silica can be derived from it by crystallizing a magnesium-rich olivine and diopsidic augite. The distinct break in lines of liquid descent for rocks containing less than 47.2% SiO_2 can be explained if the same initial magma crystallized under different physical conditions such that enstatite was the first mineral to crystallize. The removal of approximately 10 to 15% enstatite from the basalt containing 47.2% SiO_2 would result in the basanite. No enstatite phenocrysts were observed in the basanite, but if the liquid had been filter pressed enstatite could have been completely removed. Filter pressing would also account for the small size of the other phenocrysts and the lack of ultramafic nodules. Forming the basanite by the above mechanisms would account for its atypical chemical composition of high aluminum and calcium, and low magnesium and total alkalies. Thus, from the silica variation diagram it is apparent that the entire volcanic sequence may be accounted for by fractional crystallization of two parent magmas. These two magmas need not have originated from two different sources. Presnall (1969) has shown that fractional fusion of a wide variety of parent materials can produce two or more discontinuous liquids.

Presnall (1969) has distinguished two types of fusion. Fractional fusion refers to those situations in which melt is removed from the system

Reproduced with permission of the copyright owner. Further reproduction prohibited without permission.

as soon as it forms thus preventing further reaction. Equilibrium fusion refers to those situations in which the melt reacts continuously with the crystalline mass until fusion is complete. The term melt refers to the liquid only, whereas magma refers to the mixture of liquid and solid material. Partial fusion is used to describe any part less than the whole and will imply a combination of fractional fusion and equilibrium fusion. The path of changing chemical composition followed by the liquid upon fractional fusion is referred to as the liquidus fractionation path. The solidus fractionation path refers to the path of changing composition of the solid residua during fractional fusion.

Evidence for a fractional fusion origin for some Hawaiian basalts has been reported by Beeson and Jackson (1970) and Jackson and Wright (1970). In this case the liquidus fractionation path (represented by the basalts) and the solidus fractionation path (represented by xenoliths) are found in close association. Both trends are in good agreement with those predicted by a fractional fusion model. In the case of the Superstition volcanics the solidus path is not observed, but a discontinuous liquidus path is observed. Such a path can be produced by combining fractional fusion with equilibrium fusion.

The path followed by the liquid for the silicic volcanics shows a general trend of increasing silica with time. If each of these liquids were the result of fractional fusion, the reverse of this trend would be observed. The trend of increasing silica with time can be produced by fractional crystallization. This mechanism is supported by petrographic data. Most of the silicic volcanics exhibit

Reproduced with permission of the copyright owner. Further reproduction prohibited without permission.

abundant phenocrysts, zoned plagioclase and glomeroporphyritic textures. All of these features are likely to develop during fractional crystallization.

If the bimodal distribution with no intermediate members is the result of partial fusion, then the chemical data and experimental results may be combined in a semiquantitative fashion to determine the chemical composition of the source material. The following discussion is based on the experimental data of Holloway and Burnham (1971). The applicability of these calculations is dependent on the coincidence of the physical conditions used in the experimental work with the physical conditions which existed in the source region. It is believed that the total pressures and chemistry of the source region are in good enough agreement with those used in the experimental study, but that the equilibrium pressure of water and CO_2 used may be too high. Thus, the results obtained may predict a depth of origin which is too shallow.

Table 14 compares the liquid compositions obtained by partial fusion of the 1921 flow from Kilauea with the chemical compositions of the early dacites of the Superstition area. Also compared are the compositions of the calculated residua from the experimental partial fusion and the least altered of the early basalts (sample 8026). The two sets of data are in relatively good agreement. If all of the variations between the two sets of partial fusion products are attributed to a slightly different initial chemistry, then the approximate chemical composition of the source for the Superstition volcanics can be calculated (table 14). These calculations assume that all of the remaining residuum was melted after the removal of the first 29%. The erupted

Reproduced with permission of the copyright owner. Further reproduction prohibited without permission.

Reproduced with permission of the copyright owner. Further reproduction prohibited without permission.

TABLE 14

EXPERIMENTAL AND HYPOTHETICAL DATA FOR PARTIAL FUSION AT 8 KILOBARS[a]

	8092	8114	35% fusion	29% fusion	1921 basalt	Calculated residua[c]	8026[d]	Initial source[e]
SiO_2	59.53	63.62	63.2	63.0	49.2	43.6	45.7	49.71
TiO_2	0.93	0.69	1.2	1.0	2.5	3.1	1.51	1.07
Al_2O_3	17.15	18.09	20.3	19.9	13.0	10.2	15.48	15.96
FeO[b]	4.84	1.45	3.0	3.0	12.0	15.7	7.77	6.92
MgO	2.46	1.83	0.3	0.2	9.4	13.2	10.53	8.19
CaO	4.63	2.29	7.4	6.4	11.3	13.3	10.75	8.97
Na_2O	4.36	4.32	3.0	4.7	2.09	1.02	3.13	3.49
K_2O	2.62	3.46	0.9	1.0	0.49	0.28	1.01	1.48
H_2O	1.30	2.12					2.93	2.46

a. Experimental data from Holloway and Burnham (1971, Table 8). 35% fusion at 7.96 kb, 1050°C, 29% fusion 7.40 kb, 1098°C. Data for starting basaltic glass normalized to 100% after calculating total iron as FeO.

b. Total iron as FeO.

c. Calculated assuming 29% fusion.

d. Data from Fodor (1968).

e. Calculated assuming 29% 8092 and 71% 8026.

volumes in the Superstition area do not coincide with the predictions of the model. Within the Superstition area basalt constitutes less than 10% of the volcanic sequence; however, extensive areas of basalt exist to the north. Furthermore, all of the basaltic magma need not have been erupted.

This potential source material contains significantly more K_2O, Na_2O, and Al_2O_3 and significantly less CaO and FeO than the tholeiite used by Holloway and Burnham (1971). One rock fitting this chemical composition would be an amphibolite. Small changes in the physical conditions of partial fusion or in the relative amounts of derived liquids would still result in a calculated chemical composition of a possible amphibolite.

Choosing amphibolites as the source material is consistent with the seismic data. Press (1966) reports seismic velocities in amphibolites of 7.3 to 7.5 km/sec at pressures of six to ten kilobars. If the effect of increasing temperature is taken into account the velocity in amphibolites at depths of 22 to 28 km would be about 7.2 km/sec. The observed velocity in this depth range near the Superstitions is 7.0 (Warren, 1969).

The choice of amphibolites as the source material is also consistent with the strontium isotope data. Van de Kamp (1969) reports a range in Rb/Sr ratios in amphibolites of 0.03 to 0.33. As mentioned earlier, if the source area is assumed to be 2.5 to 2.7 billion years old, then it must have a Rb/Sr ratio of 0.05 to account for the volcanic rocks with initial ratios of 0.7050 to 0.7055. Amphibolites are likely to have high alkali contents and low Rb/Sr ratios because amphiboles tend to strongly fractionate against Rb relative to K (Hart and Aldrich, 1967).

Reproduced with permission of the copyright owner. Further reproduction prohibited without permission.

For an amphibole containing up to 1.5%K, the Rb/K fractionation between the amphibole and whole rock is about 5. Thus, if most of the alkalies are in the amphibole, an amphibolite, especially one at high pressures, would be expected to have a low Rb/Sr ratio. Finally, the partial melting of an amphibolite would provide a better source of water than would other materials which also fit with the Rb/Sr, seismic, and chemical limitations.

Deriving both the mafic and silicic volcanics from one source is consistent with the strontium isotope data in that several rocks from both suites have similar initial ratios (table 10). Local variations of the Rb/Sr ratio in the source region could account for the variation of initial ratios between 0.7055 and 0.7063. That this variation exists in the source region is supported by the two basanite flows which have different initial ratios. Because these rocks contain relatively large amounts of strontium, and because their chemistry is greatly different from that of the potential source of radiogenic strontium (crustal rocks), it would be difficult to contaiminate one basanite more than the other without producing a corresponding change in chemical compositions.

In summary, it is proposed that the volcanic magmas resulted from the partial melting of an amphibolite to produce a melt similar to the quartz-poor dacite. This liquid was then removed from the system during the melting break caused by the disappearance of amphibole. The continued addition of heat caused the temperature to rise to a point where the residuum was melted to produce the basalts. Yoder (1971) has suggested that the hiatus in melting would probably be a few thousand years which should be sufficient time to separate the first liquid.

Reproduced with permission of the copyright owner. Further reproduction prohibited without permission.

The separated silicic melt began to undergo fractional crystallization. An estimate of the physical conditions of the magma chamber at this time can be obtained from oxygen isotope geothermometry and phase equilibria. The temperature of crystallization for the Superstition Tuff has been determined at $990^{\circ} \pm 20^{\circ}C$ (table 12). The pressure during crystallization can be estimated from the system Q-Or-Ab.

If the bulk of normative compositions of these rocks are plotted on a Q-Or-Ab diagram (fig. 14), they fall between the 2 and 3 kb isobars of Tuttle and Bowen (1958). However, these are phase boundaries on which the liquidus would be when crystallizing at equilibrium and furthermore they are for water-saturated magmas. The normative, modal and partial chemical data (tables 5,6 and 13) for the rocks and mineral phases can be used to calculate an approximate liquid composition. The amount of plagioclase is calculated by multiplying 0.7 times the modal amount of plagioclase plus 0.25 times the modal amount of sanidine. The potassium feldspar is calculated by multiplying the modal amount of sanidine by 8.75. These data plus modal quartz are then normalized to 100% and plotted on the Q-Or-Ab diagram as the phenocryst mode. The liquid composition is then obtained by using the crystal composition, the normative composition, the modal percent groundmass, and the lever rule. The results show that all three members of the Superstition Tuff must have crystallized at pressures greater than 3 kb if the magma was water-saturated and crystallizing at equilibrium.

The uniqueness of conclusions drawn using these calculations and the Q-Or-Ab system are limited by the unknown water content, the fact

Reproduced with permission of the copyright owner. Further reproduction prohibited without permission.

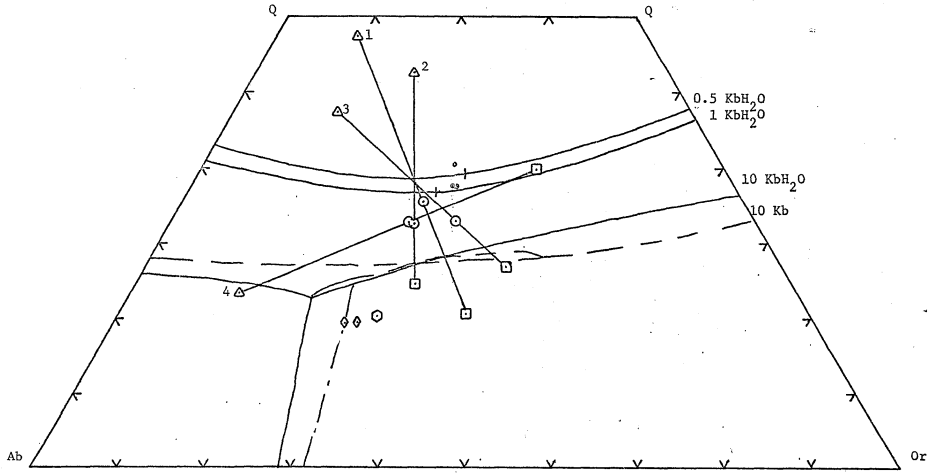

Figure 14 - The system Q-Or-Ab showing phase relationships at 0.5, 1, and 10 Kb water saturated projected on the anhydrous base of the tetrahedron and water undersaturated at 10 Kb (after Luth, 1969). 1 = ave. Siphon Draw Mbr., 2 = ave. Dogie Spring Mbr., 3 = ave. Canyon Lake Mbr., and 4 = ave Apache Leap Tuff (data from Peterson, 1961). Circle = whole rock norm, triangle = phenocryst mode as explained in the text, square = calculated liquid composition, hexagon = calculated normal dacite liquid composition, diamond = calculated quartz poor dacite liquid composition, and dot = whole rock Geronimo Head rhyolite ash flow norm (data from Fodor, 1968).

Reproduced with permission of the copyright owner. Further reproduction prohibited without permission.

that this sytem represents only about 90% of the rock, and the assumption that the rocks used represent a quenched equilibrium assemblage. Lipman (1966) has suggested that only those rocks which contain normative Q + Or + Ab greater than 95% will closely approximate the experimental systems. The effect of An greater than 5% will probably shift the eutectic in the Q-Or-Ab projection a little towards the Q-Or sideline (Whitney, personal communication, 1971).

There is currently a growing amount of evidence that the beginning of crystallization in a silicic magma is under conditions of water undersaturation. The fractional fusion model proposed for the derivation of the magma implicitly assumes a water undersaturated environment. It is unlikely that a significant amount of water would be added between the time of derivation and the beginning of crystallization. The effect of water undersaturation is to shift the eutectic towards the Q-Or sideline, as predicted by Luth (1969).

The liquid compositions of the three members of the Superstition Tuff (fig. 14) plot to the right of the 10 kb quaternary eutectic (projected on the anhydrous base), but to the left of the nearly anhydrous ternary eutectic (eutectics from Luth, 1969, p. 337). This suggests that these three members crystallized at relatively high pressures and that the magmas were undersaturated with respect to water. The Siphon Draw Member whose liquid plots lowest on the diagram exhibits the least quartz resorbtion and may well be the most accurate representation of the liquid composition. Furthermore, its modal percent of phenocrysts is determined from a larger number of densely welded specimens and is therefore a better estimate of the volume percent phenocrysts in the melt.

Reproduced with permission of the copyright owner. Further reproduction prohibited without permission.

The relatively high total pressure during crystallization suggested in the above discussion is supported by the isotope studies. If the approximate temperature determined by oxygen isotope work is accepted, then the melt could not have been in contact with the granitic basement for any great length of time without becoming enriched in Sr^{87}. From the earlier discussion regarding the depth to the base of the granitic basement, it appears likely that the quartz latite ash flows started crystallizing at depths in excess of 22 kilometers.

During the ascent of this magma to the surface (in a closed system) the activity of water would increase and the temperature of the melt could decrease (Luth, 1969). The development of a free aqueous fluid phase would provide the driving force necessary for ash-flow eruption. The decrease in temperature is in accord with that observed by oxygen isotope geothermometry. Furthermore, any re-equilibration of the melt with the crystals at lower pressures would result in the resorbtion of quartz which is also observed.

The data for the Apache Leap Tuff are also plotted on figure 14. Although these are uncorrected for the Ab in the sanidine and the An in the plagioclase, the calculated liquid suggests a much lower total pressure during crystallization. This lower pressure is probably responsible for the contrasting phenocryst percentages in the Superstition Tuff and Apache Leap Tuff. If the Apache Leap Tuff did crystallize at low total pressure, its magma was probably in contact with the granitic basement for an extended period of time and therefore could have become enriched in Sr^{87}. Preliminary measurements at the base and top of this tuff show Sr^{87}/Sr^{86} to be greater than 0.7110.

Three analyses of the Geronimo Head ash flows (fig. 14) also indicate crystallization under low total pressure. In this case the

Reproduced with permission of the copyright owner. Further reproduction prohibited without permission.

whole rock Q-Or-Ab ratios are nearly identical to the phenocryst ratios. Furthermore, the total phenocryst content is less than 10%. Therefore the value for the whole rock ratios are essentially the same as for the liquid. The total pressure appears to be in the range of 500 to 1000 bars. Thus, as suggested by the isotope data, the Geronimo Head ash flows and the Superstition Tuff crystallized in different environments.

The last volumetrically important unit is the older dacite. For this unit only 64% to 77% of the rock is represented by the Q-Or-Ab system. Furthermore, none of the analysed samples were crystallizing at the eutectic as evidenced by their lack of sanidine or sanidine plus quartz. However, sample 8114 must have been crystallizing on a phase boundary as it contains plagioclase and quartz. Its liquidus composition (fig. 14) must lie to the left of the eutectic.

The proximity of the quartz-poor dacite liquids to this liquid suggests that all of the older dacite complex crystallized at relatively high pressures and in a water undersaturated environment. This conclusion is again supported by the low Sr^{87}/Sr^{86} initial ratio for the unit.

The physical conditions of crystallization for the Superstition volcanics are not the same for each unit. Most of the volcanics appear to have crystallized at relatively high temperatures and high pressures. During their ascent to the surface these units have undergone varying degrees of phase re-equilibration. All of the silicic units exhibit resorbed quartz and appear to have crystallized biotite and perhaps hornblende only after the initially high temperature was

Reproduced with permission of the copyright owner. Further reproduction prohibited without permission.

lowered.

The Geronimo Head Formation appears to have had the longest residence in the lower pressure and lower temperature environment. Its quartz has been nearly entirely resorbed, the oxygen isotope fractionations have readjusted to the lower temperature, and the strontium has become greatly enriched in Sr^{87}.

The rhyolite dome from which AP-219 and T-111 were collected appears to have had a similar genesis. Its quartz has also been largely resorbed, the oxygen isotope fractionations for several mineral pairs have readjusted to lower temperatures, and the strontium has become greatly enriched in Sr^{87}.

Reproduced with permission of the copyright owner. Further reproduction prohibited without permission.

STRUCTURAL EVOLUTION

The structures in the Superstition region record at least three, and possibly four, tectonic events. The oldest faulting appears to have affected only the Precambrian basement. The record of this event is preserved by brecciated and altered zones in the granitic basement which do not extend up into the Tertiary rocks, and by small down-dropped blocks of the Precambrian metamorpphics within the granite. On the basis of field evidence, this faulting can only be bracketed between 1.4 billion years and the middle Tertiary. These faults trend northwest and may have had an effect on a northwest trending graben zone which controls three volcano-tectonic subsidence blocks: 1) The Willow Springs cauldron; 2) The Black Mesa cauldron; and 3) The Florence Junction cauldron (Sheridan and others, 1970). Some of this faulting may be related to larimide uplift which is recorded by fission-track ages in the Precambrian apatite (table 8).

The second tectonic event is attributed to Basin and Range faulting, which probably started just before the volcanism or during its early stages. Evidence for this age assignment is weak, but it appears that the arkosic conglomerate and sandstone and the early basalt were spread over a large area (Sell, 1968) with moderate topographic relief. Had this topography existed during the succeeding ash-flow eruptions, the Superstition Tuff would have spread over a great distance. However, the Superstition Tuff occurs as thick accumulations

Reproduced with permission of the copyright owner. Further reproduction prohibited without permission.

in what must have been topographic depressions. These depressions appear to have been long north-south basins because the Superstition Tuff does crop out 40 km to the south in the San Tan Mountains (Sheridan, personal communication, 1971).

Peterson (1961) found only the Apache Leap Tuff in the Superior region and identified the source region as Haunted Canyon. The centers of the Haunted Canyon cauldron and the Superstition caldera are separated only by 30 km and their outer limits are separated by only 10 km. Both tuffs attain a maximum thickness of approximately 670 m. For two such thick ash-flow tuffs to be so closely related in space and time implies either a large topographic barrier between them at the time of eruption or subsequent strike slip faulting which has brought the two much closer together than they were at the time of eruption.

The Arizona State Geologic Map (Wilson and others, 1969) shows no evidence for any extensive strike slip movement between the two tuffs, but a topographic high is suggested by a block of Precambrian granite. This block could have become a topographic high after the deposition of the arkosic conglomerate. The up-faulting of this block may then be part of the Arizona Basin and Range faulting which has been dated in southern Arizona as beginning at 28 to 25 million years ago (Damon, 1968). This episode appears to become progressively younger to the north. In the Prescott region of Arizona the Basin and Range events may be as young as early Pliocene (Damon, 1968).

The Basin and Range faulting in the Superstition region appears to be predated by the older basalts and the early dacites, and postdated by the first ash flows of the Superstition Tuff. The beginning of this faulting in the Superstition area is then bracketed between 29 and 24 million years ago. This age assignment is in agreement with

Reproduced with permission of the copyright owner. Further reproduction prohibited without permission.

that determined in southern Arizona, but does not agree with the predicted northward decrease in age of Damon (1968). However, it does agree with the Basin and Range faulting period in northern New Mexico which is believed to have started 28 to 25 million years ago (Lipman, personal communication, 1971).

The end of the Basin and Range faulting episode in the Superstition area overlaps with a volcano-tectonic event. Therefore, the duration of Basin and Range faulting cannot be determined. The Superstition Tuff has been faulted out between the Superstition and San Tan Mountains which suggests that Basin and Range faulting could be as young as 15 m.y.

Mapping in the Superstition area (plate 1) and reconnaissance mapping in adjacent areas indicate the Superstition Mountain block is the central core (or part of the central core) of a large caldera. The outer limits of this caldera are crudely outlined by the distribution of the late stage glassy domes and lavas. These form a ring with an approximate diameter of 30 km. The inner limits of the ring fracture zone are roughly defined by the older dacite complex. This ring of domes may be the surface expression of either a ring dike or a cone sheet. The deformation pattern within the ring fracture zone consists of subsidence, tilting and rotation of large blocks. The detailed structure and morphology of the Superstition caldera have been largely obscured by subsequent formation of the smaller cauldrons already mentioned. Detailed mapping in the vicinity of Goldfield (plate 1) shows a progressive inward deformation and rotation of large blocks (one to two km in diameter) with dips steepening towards the caldera core. One block which may have also been affected by cauldron formation

Reproduced with permission of the copyright owner. Further reproduction prohibited without permission.

is overturned. Similar features, although not shown in detail in plate 1, exist to the south of the Superstition Mountain block.

Faults and dikes in the ring fracture zone are approximately tangential or radial to the Superstition block. Similar structures are observed to the east of the caldera, but here the blocks are predominantly Precambrian metamorphics which could have formed before the caldera. However, because the volcanics adjacent to these metamorphic blocks are also complexly faulted, it is believed that the faulting in the Precambrian terrain is due to caldera formation. To the north the ring fracture zone is largely occupied by quartz latite domes and lavas which in most cases bury the faults of the ring fracture zone.

The stable volcanic plateau outside the caldera covered by the Superstition Tuff is not preserved in the area mapped, but may exist to the north and to the northeast (Sheridan, personal communication, 1970). Volcanic rocks with dips less than 20° do surround the caldera, but these may post-date caldera formation.

The collapse of the Superstition caldera was followed by intrusion and extrusion of domes and lavas in both the ring fracture zone and under the central core. This resulted in a Valles-type resurgent caldera (Smith and others, 1961). The flat-lying resurgent core is now preserved in the Superstition Mountain block. The maximum former extent of this core has been obscured to the northwest by subsequent cauldron formation. To the northeast the resurgent core has been deeply eroded exposing a granophyric porphyry which is similar in chemistry, mineralogy and strontium isotopes to the Superstition Tuff (sample AP-212). This dome (plate 1) is believed to represent the resurgent

Reproduced with permission of the copyright owner. Further reproduction prohibited without permission.

magma of the Superstition caldera. The probably extent of the original resurgent central core is shown in figure 1.

The fourth and final tectonic event is the formation of the smaller cauldrons. This event probably overlaps with the formation of the larger caldera and with the Basin and Range faulting. Elements of all three cauldrons are preserved within the area mapped, but only the Black Mesa cauldron is completely exposed in the mapped area.

The northwestern edge of the Florence Junction cauldron overlaps with the ring fracture zone of the Superstition caldera along the southeastern part of the mapped area (fig. 1). In the region of Apache Gap (northwestern edge of plate 1) the faulting associated with two cauldron ring fracture zones (Black Mesa and Willow Springs) overlaps in the ring fracture zone of the Superstition caldera causing great structural complexity.

The stable volcanic plateau, the ring fracture zone and the resurgent core of the Black Mesa cauldron can be approximately located (fig. 1). The morphology of these features is controlled and partly obscured by the relationship of the cauldron to the older tectonic events. To the west and north the Black Mesa cauldron ring fracture zone overlaps the Superstition caldera ring fracture zone and its exact limits are therefore difficult to locate. To the east and south the ring fracture zone of the Black Mesa cauldron is a relatively narrow zone within the resurgent central core of the Superstition caldera. The northwest elongation of the cauldron is attributed to the pre-existing graben zone and the Superstition caldera.

The ring fracture zone of Black Mesa is characterized by radial and tangential faulting. The tangential faults are best displayed

Reproduced with permission of the copyright owner. Further reproduction prohibited without permission.

to the south and east. A graben zone with an approximate displacement of 670 meters in the southern ring fracture zone separates Black Mesa from the Superstition Mountain block. To the west several parallel high-angle normal faults down-drop the central core at least 350 meters. Down-dropping of the central core to the north and west is believed to be of the same order of magnitude. However, the only well displayed tangential faults to the north are in the graben zone which bounds Canyon Lake and these may be associated with the Superstition caldera. Radial faulting is well displayed on the north and west sides of Black Mesa and is particularly well displayed in the southeast corner.

The stable volcanic plateau can be seen on the northeast, east, southwest and southern edges of the cauldron where units are nearly flat-lying. To the west the stable plateau is missing. To the northwest the stable volcanic plateau overlaps with the Willow Springs cauldron. To the southwest it has been removed by erosion.

Most of the resurgent central core is capped by basanite and includes Black Mesa and Black Top Mesa. Although the two are separated by an erosional gap (fig. 7) their tops are concordant, indicating that they have acted as a single structural block. The faults bounding Black Mesa are antithetic to the dip of the units which is typical of Basin and Range faulting, but because these faults are up-thrown on the Black Mesa side, they are attributed to resurgence of the central core. The minor faults within the central core are also attributed to magma resurgence.

The various morphological features associated with the Black Mesa cauldron can be seen in figures 7 and 15. The basanite capped

Reproduced with permission of the copyright owner. Further reproduction prohibited without permission.

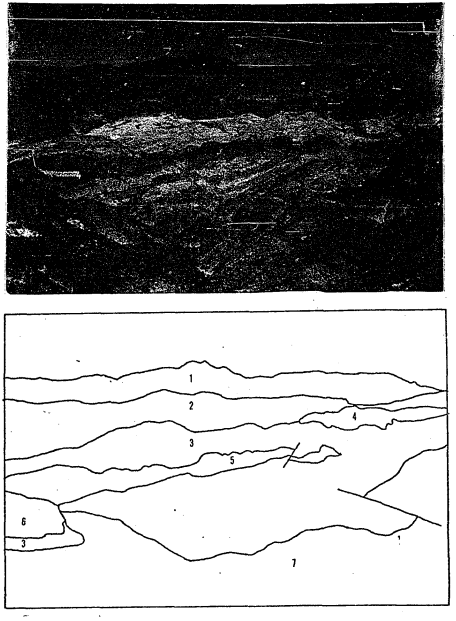

Figure 15 - Photograph of the northern ring fracture zone of the Black Mesa cauldron. 1 = Precambrian basement, 2 = flat lying volcanic units, 3 = north-dipping sequence of rhyolite ash-flows and lahars, 4 = quartz latite dome, 5 = quartz latite dike, 6 = quartz latite lava, and 7 = older dacite dome.

Reproduced with permission of the copyright owner. Further reproduction prohibited without permission.

resurgent core can be seen in figure 7 with a deep fault controlled canyon behind it (west side). The stable volcanic plateau can be seen in the middle distance but is broken in the far distance where it occupies the Superstition caldera ring fracture zone.

Down-dropping along the eastern margin appears to have been more active during the formation of the cauldron as evidenced by the general eastward thickening of the Geronimo Head Formation (fig. 7). The eastward dip of Black Mesa could have developed during differential subsidence, but could have been accentuated by differential uplift. To the near side of Black Mesa (fig. 7) lies a topographic low which is occupied by a graben zone. Figure 15 shows the typical appearance of the well developed ring fracture zone along the northern boundary of Black Mesa. The Geronimo Head Formation is steeply dipping, strongly faulted and intruded by multiple quartz latite dikes and domes.

The sequence of cauldron formation is believed to be: 1) The Willow Springs cauldron; 2) The Black Mesa cauldron; and 3) The Florence Junction cauldron. Each of these cauldrons is filled with rhyolite ash of the Geronimo Head Formation and it is therefore likely that each is an eruptive center for the Geronimo Head Formation. The Dogie Spring Member of the Superstition Tuff also fills a depression and may directly overlie its vent area.

The overall structure and morphology observed in the Superstition volcanic area is typical of other described nested calderas. Luedke and Burbank (1968) have described a nearly identical structure where the Silverton and Lake City calderas lie within the San Juan volcano-tectonic depression. The San Juan depression is controlled by earlier faulting and is elongate in a northeasterly direction. This was

Reproduced with permission of the copyright owner. Further reproduction prohibited without permission.

followed by the nearly contemporaneous formation of the Silverton and Lake City calderas which collapsed and then formed resurgent cores of the Valles type. Finally, late stage basalts were extruded.

Reproduced with permission of the copyright owner. Further reproduction prohibited without permission.

SUMMARY

The rocks of the Superstition region record three periods of igneous activity. The two older periods consist of pluton emplacement during the Precambrian. The older pluton yields a Rb-Sr age of 1540 ± 84 m.y., but computer calculations indicate a redistribution of strontium. The age obtained is therefore likely to be too young and the unit is therefore correlated with the Madera quartz diorite (1660 m.y.). The redistribution of strontium is probably due to the emplacement of the younger pluton which yields a Rb-Sr age of 1395 ± 45 m.y. This pluton is correlated with the Ruin granite.

Volcanism started in the Superstition region during the middle Tertiary with the extrusion of a thin alkali olivine basalt into a large basin in which arkosic conglomerates and sandstones were being deposited. This was followed by the intrusion and extrusion of a ring of dacitic domes dated at 29.0 m.y. The early dacites were quartz-poor and were followed by the extrusion of more voluminous quartz-rich dacites.

The last phases of dacite doming were contemporaneous with the eruption of the Siphon Draw Member of the Superstition Tuff (24.4 m.y.). Collapse of the Superstition caldera is believed to have been in part contemporaneous with the extrusion of the Siphon Draw Member, thereby accounting for the thick accumulation of tuff within the caldera. The total amount of collapse may have been as much as 800 meters.

Reproduced with permission of the copyright owner. Further reproduction prohibited without permission.

Final collapse of the Superstition caldera was accompanied by the eruption of the first Geronimo Head ash-flow and closely followed by the extrusion of quartz latite domes and lavas (21 m.y. and 20 m.y.). This quartz latite magma resurgence probably up-lifted the core of the Superstition caldera. Successive rhyolite ash-flows caused collapse of the smaller cauldrons. This phase continued until about 15 million years ago and was accompanied and followed by more quartz latite domes, lavas, ash flows and mafic lavas. The smaller cauldrons were probably formed throughout this period.

Various episodes of magma resurgence uplifted the central cores of each of the cauldrons. Doming also occurred within the ring fracture zone of the Superstition caldera in the region now occupied by the Dogie Spring Member of the Superstition Tuff. Volcanism came to a close between 10 and 15 million years ago with the extrusion of the basalt of Canyon Lake and the formation of small rhyolite dikes and domes around the outer margins of the Superstition caldera ring fracture zone.

The Superstition volcanics resulted from magma (s) derived below the base of the granitic crust as indicated by the relatively low Sr^{87}/Sr^{86} initial ratios. Both the silicic and mafic volcanics can be related to a common source as shown by their similar Sr^{87}/Sr^{86} ratios and recent experimental studies of partial fusion. Once formed, the two "parent magmas" differentiated yielding two discontinuous, but cogenetic suites.

Most of the volcanics started to crystallize at high temperatures and pressures as indicated by the system Q-Or-Ab-H_2O, and oxygen isotope geothermometry. These magmas were undersaturated with respect to water.

Reproduced with permission of the copyright owner. Further reproduction prohibited without permission.

During their ascent to the surface these magmas underwent minor crystal-melt-re-equilibration. This is indicated by resorbed quartz crystals and by some rocks containing resorbed plagioclase crystals. The ascent of the magma was apparently accompanied by a decrease in temperature which resulted in the crystallization of biotite and possibly hornblende. This is indicated by oxygen isotope geothermometry. Prior to eruption the upper portions of the magma column became progressively contaminated as indicated by Sr^{87} enrichment at the base of the quartz latite ash flows.

The magma responsible for the Geronimo Head Formation appears to have had a much longer residence in the crust at low pressures and temperatures as evidenced by its greater enrichment in Sr^{87}, lower oxygen isotope temperatures, and liquidus composition in the system Q-Or-Ab-H_2O. The lower crystallization pressures for this formation suggest a magma chamber depth of 2 to 5 km.

The following model is proposed as being consistent with the data and therefore permissible. The silicic magma was generated by approximately 30% partial fusion of an amphibolite lower crust. This liquid was then separated from its source during a melting hiatus and moved to a higher level in the lower crust. Continued melting of the source resulted in a basaltic liquid which was differentiated and extruded. Extrusion from this source then continued intermittently throughout the formation of the Superstition volcanic field.

Part of the separated silicic magma was then tapped off and intruded as ring dikes or possibly cone sheets which have their surface expression in the early quartz-poor dacites. Continued crystallization

Reproduced with permission of the copyright owner. Further reproduction prohibited without permission.

and differentiation resulted in the extrusion of the quartz-rich dacites. As crystallization continued a large volume of quartz latite magma moved up into the crust forming a temporary laccolith or similar intrusive body.

This intrusion must have domed the Superstition area and the roof of the magma chamber ruptured (possibly along the early cone sheet fractures). The fracturing of the roof of the magma chamber was accompanied by the extrusion of quartz latite ash flows and collapse. This sequence was repeated at least nine times accounting for the nine flows of the Siphon Draw Member.

The liquid remaining in the magma chamber continued to differentiate largely by fractional crystallization until increasing water pressure triggered the eruption of the first Geronimo Head ash flow. Replenishment of the magma chamber from the lower crust resulted in the Dogie Spring Member, collapse, and more rhyolite ash. This cycle was apparently started a third time with the extrusion of the Canyon Lake Member.

Throughout the period of ash flow and collapse, volatile-poor magmas were intruded along the fractures which accompanied collapse. Final resurgence of the most differentiated magma from the lower crust produced a ring of glassy rhyolitic domes.

The above discussion of magma derivation and crystallization is believed to be generally applicable to the Basin-Range province. However, local variations may change the details of the proposed model.

Reproduced with permission of the copyright owner. Further reproduction prohibited without permission.

REFERENCES CITED

Barth, T.F.W., 1962, Theoretical petrology; second edition: New York, John Wiley and Sons, 416 p.

Beeson, M.H., and Jackson, E.D., 1970, Origin of the garnet pyroxenite xenoliths at Salt Lake Crater, Oahu: Mineralog. Soc. America, Spec. Paper, 3, p. 95-112.

Bikerman, M., 1968, The geology of the Roskruge Mountains: Arizona Geol. Soc. Southern Arizona Guidebook III, p. 183-191.

Bowen, N.L., 1928, The evolution of igneous rocks: Princeton, New Jersey, Princeton Univ. Press, 334 p.

Burri, C., Parker, R.L., and Wenk, E., 1967, Die optische orientierung der plagioklase: Basel und Stuttgart, Burkhauser Verlag, 334 p.

Christiansen, R.H., Lipman, P.W., Orkild, P.P., and Byers, A.M., Jr., 1965, Structure of Timber Mountain Caldera, southern Nevada, and its relationship to Basin-Range structure: U.S. Geol. Survey Prof. Paper 525-B, p. B43-B48.

Craig, H., 1961, Isotopic variations in meteoric waters: Science, V. 133, no. 3465, p. 1702-1703.

Daly, R.A., 1933, Igneous rocks and depths of the earth: New York, McGraw-Hill, 563 p.

Damon, P.E., and Bikerman, M., 1964, Potassium-argon dating of post-Laramide plutonic and volcanic rocks within the Basin and Range Province of southern Arizona and adjacent areas: Arizona Geol. Soc. Digest, V. 7, p. 63-78.

Damon, P.E., 1968, Application of the potassium-argon method to the dating of igneous and metamorphic rocks within the Basin Ranges of the southwest: Arizona Geol. Soc. Southern Arizona Guidebook III, p. 7-20.

____, 1969, Correlation and chronology of ore deposits and volcanic rocks: U.S. Atomic Energy Comm., Annual Progress Report No. COO-689-120, 90 p.

Dasch, E.J., 1969, Strontium isotope disequilibrium in a porphyritic alkali basalt and its bearing on magmatic processes: Jour. Geophys. Research, V. 74, p. 560-565.

Reproduced with permission of the copyright owner. Further reproduction prohibited without permission.

Doe, G.R., Hedge, C.E., and White, D.E., 1966, Preliminary investigation of the source of lead and strontium in deep geothermal brines underlying the Salton Sea geothermal area: Econ. Geology, V. 61, no. 3, p. 462-483.

Doe, B.R., 1968, Lead and strontium isotopic studies of Cenozoic volcanic rocks in the Rocky Mountain region - a summary: Colorado School Mines Quart., V. 63, no. 3, p. 149-174.

Doe, B.R., Lipman, P.W., and Hedge, C.E., 1969, Radiogenic tracers and the source of continental andesites: a beginning at the San Juan Volcanic Field, Colorado, in Proceedings of the Andesite Conference, International Upper Mantle Project Scientific Report 16: Oregon Dept. Geology Mineral Industries Bull. 65, p. 143-149.

Doe, B.R., Lipman, P.W., Hedge, C.E., and Kurasawa,Hajime, 1969, Primitive and contaminated basalts from the southern Rocky Mountains, U.S.A.: Contr. Mineralogy and Petrology, V. 21, no. 2, p. 142-156.

Elston, W.E., 1965, Rhyolite ash-flow plateaus, ring-dike complexes, calderas, lopoliths, and moon craters: New York Acad. Sci. Annals, V. 123, p. 817-842.

Ewart, A., and Stipp, J.J., 1968, Petrogenesis of the volcanic rocks of the central North Island, New Zealand, as indicated by a study of Sr^{87}/Sr^{86} ratios, and Sr, Rb, K, U, and Th abundances: Geochim. et Cosmochim. Acta, V. 32, no. 7, p. 699-736.

Faure, G., and Hurley, P.M., 1963, The isotopic composition of strontium in oceanic and continental basalts: application to the origin of igneous rocks: Jour. Petrology, V. 4, no. 1, p. 31-50.

Fernandez, L.A., Jr., and Enlows, H.E., 1966, Petrology of the Faraway Ranch Formation, Chiricahua National Monument, Arizona: Geol. Soc. America Bull., V. 77, p. 1017-1030.

Fisher, R.V., 1960, Classification of volcanic breccia: Geol. Soc. America Bull. V. 71, p. 970-982.

Fodor, R.V., 1968, Petrology and petrography of the volcanic rocks in the Goldfield Mountains, Arizona: unpub. M.S. Thesis, Arizona State University, 66 p.

Hamilton, E.I., 1963, The isotopic composition of strontium in the Skaegaard intrusive, East Greenland: Jour. Petrology, V. 4, no. 3, p. 483-491.

Hart, S.R., and Aldrich, L.T., 1967, Fractionation of potassium/rubidium by amphiboles: implications regarding mantle composition: Science, V. 155, no. 3760, p. 325-327.

Reproduced with permission of the copyright owner. Further reproduction prohibited without permission.

Hedge, C.E., and Walthall, F.G., 1963, Radiogenic strontium-87 as an index of geologic processes: Science, V. 140, no. 3572, p. 1214-1217.

Hedge, C.E., 1966, Variations in radiogenic strontium found in volcanic rocks: Jour. Geophy. Research, V. 71, no. 24, p. 6119-6126.

Holloway, J.R., and Gurnham, W.C., 1971, Melting relations of basalt with equilibrium water pressure less than total pressure: Jour. Petrology, in press.

Jackson, E.D., and Wright, T.L., 1970, Xenoliths in the Honolulu volcanic series, Hawaii: Jour. Petrology, V. 11, p. 405-430.

Keil, K. and Fredrikson, K., 1964, The Fe, Mg, and Ca distribution in co-existing olivines and rhombic pyroxenes: Jour. Geophy. Research, V. 69, no. 16, p. 3487-3515.

Kokalis, 1971, Terraces of the lower Salt River Valley, Arizona: Unpub. M.S. Thesis, Arizona State University, p.

Krieger, M.H., 1968, Ash-flow tuff in the northern Galiuro Mountains, Pinal County, Arizona (abs.), in program with abs. Cordilleran Sec.: Geol. Soc. America, abs. with programs, Cordilleran Sec.

Lipman, P.W., 1965, Chemical composition of glassy and crystalline volcanic rocks: U.S. Geol. Survey Bull. 1201-D, p. D1-D24.

_____, 1966, Water pressures during differentiation and crystallization of some ash-flow magmas from sourthern Nevada: Am. Jour. Sci., V. 264, p. 810-826.

Lipman, P.W., and Van Alstine, R.E., 1969, Retention of alkalies by calc-alkalic rhyolites during crystallization and hydration: Am. Mineralogist, V. 54, p. 286-291.

Lipman, P.W., Steven, T.A., and Mehnert, H.H., 1970, Volcanic history of the San Juan Mountains, Colorado, as indicated by potassium-argon dating: Geol. Soc. America Bull. V 81, p. 2329-2352.

Livingston, D.E., and Damon, P.E., 1968, The ages of stratified Precambrian rock sequences in central Arizona and northern Sonora: Canadian Jour. Earth Sci., V. 5, p. 763-772.

Luedke, R.G., and Burbank, W.S., 1968, Volcanism and cauldron development in the western San Juan Mountains, Colorado: Colorado School Mines Quart., V. 63, no. 3, p. 175-208.

Luth, W.C., 1967, Studies in the system $KAlSiO_4$ - Mg_2SiO_4 - SiO_2-H_2O: I, inferred phase relations and petrologic applications: Jour. Petrology, V. 8, p. 372-416.

_____, 1969, The systems $NaAlSi_3O_8$ - SiO_2 and $KalSi_3O_8$ to 20 Kb and the relationship between H_2O content, P_{H_2O} and P_{total} in granitic magmas: Am. Jour. Sci., Schairer Vol. 267-A, p. 325-341.

Reproduced with permission of the copyright owner. Further reproduction prohibited without permission.

Mackin, J.H., 1960, Structural significance of Tertiary volcanic rocks in southwestern Utah: Am. Jour. Sci., V. 258, p. 81-131.

Marjaniemi, D., 1968, Tertiary volcanism in northern Chiricuhua Mountains, Cochise County, Arizona: Arizona Geol. Soc. Southern Arizona Guidebook III, p. 209-214.

Mayo, E.B., 1968, The history of geologic investigation in the Tucson Mountains, Pima County, Arizona: Arizona Geol. Soc. Southern Arizona Guidebook III, p. 155-170.

McIntyre, G.A., Brooks, C., Compston, W., and Turek, A., 1966, A statistical assessment of Rb-Sr isochrons: Jour. Geophys. Research, V. 71, p. 5459-5468.

Moorbath, S., and Bell, J.D., 1965, Strontium isotope abundance studies and rubidium-strontium age determination on Tertiary igneous rocks from the Isle of Skye, North-West Scotland: Jour. Petrology, V. 6, no. 1, p. 37-66.

Naeser, C.W., and McKee, E.H., 1970, Fission-track and K-Ar ages of Tertiary ash-flow tuffs, North-central Nevada: Geol. Soc. America Bull. V. 81, p. 3375-3384.

Noble, D.C., and Hedge, C.E., 1969, Sr^{87}/Sr^{86} variations within individual ash-flow sheets, in Geological Survey Research 1969: U.S. Geol. Survey Prof. Paper 650-C, p. C133-C139.

O'Conner, J.T., 1965, A classification for quartz-rich igneous rocks based on feldspar ratios: U.S. Geol. Survey Prof. Paper 525-B, p. B79-B84.

O'Neil, J.R., and Clayton, R.N., 1964, Oxygen isotope geothermometry: Isotopic and cosmic chemistry (ed. H. Craig, S.L. Miller, and G.J. Wasserburg), Amsterdam, North-Holland Publ. Co., p. 157-168.

Pankhurst, R.J., 1969, Strontium isotope studies related to petrogenesis in the Caledonian basic igneous province of NE Scotland: Jour. Petrology, V. 10, p. 115-143.

Peterman, Z.E., Hedge, C.E., and Braddock, W.A., 1968, Age of Precambrian events in the northeastern Front Range, Colorado: Jour. Geophys. Research, V. 73, no. 6, p. 2277-2296.

Peterson, D.W., 1961, Dacite ash-flow sheet near Superior and Globe, Arizona: Unpub. Ph.D. dissertation, Stanford University, California, 130 p.

_____, 1966, Geology of Picket Post Mountain, northeast Pinal County, Arizona: Arizona Geol. Soc. Digest, V. 8, p. 159-176.

_____, 1969, Geologic Map of the Superior quadrangle, Arizona: U.S. Geol. Survey Quad. Map GQ818.

Reproduced with permission of the copyright owner. Further reproduction prohibited without permission.

_____, 1970, Ash-flow deposits - their character, origin and significance: Jour. Geol. Education, V. XVIII, no. 2, p. 66-76.

Presnall, D.C., 1969, The geometrical analysis of partial fusion: Am. Jour. Sci., V. 267, p. 1178-1194.

Press, Frank, 1966, Seismic velocities: in Handbook of Physical Constants: Geol. Soc. America Mem. 97, p. 195-218.

Pushkar, P.D., 1970, Sr^{87}/Sr^{86} ratios of volcanic rocks on and near the Colorado Plateau: U.S. Atomic Energy Comm., Annual Progress Report No. COO-689-130, p. 22-27.

Ransome, R.L., 1903, Geology of the Globe Copper district, Arizona: U.S. Geol. Survey Prof. Paper 12, 168 p.

Ratte, J.C., and Steven, T.A., 1967, Ash flows and related volcanic rocks associated with the Creede Caldera, San Juan Mountains, Colorado: U.S. Geol. Survey Prof. Paper 524H, p. H2-H58.

Rittmann, A., 1962, Volcanos and their activities, second ed; New York, Interscience, 305 p.

Ross, C.S., and Smith, R.L., Ash-flow tuffs; their origin, geologic relations, and identification: U.S. Geol. Survey Prof. Paper 366, 81 p.

Rutherford, M.J., 1969, An experimental determination of iron biotite-alkali feldspar equilibria: Jour. Petrology, V. 10, p. 381-408.

Sell, J.D., 1968, Correlations of some post-Laramide Tertiary units Globe (Gila County) to Gila Bend (Maricopa County), Arizona: Arizona Geol. Soc. Southern Arizona Guidebook III, p. 69-74.

Sheridan, M.F., 1968, Volcanic geology along the western part of the Apache Trail, Arizona: Arizona Geol. Soc. Southern Arizona Guidebook III, p. 227-229.

Sheridan, M.F., and Fodor, R.V., 1968, Origin of the silicic ash-flow tuffs and lavas in the Goldfield Moutains, Arizona (abs.), in Abstracts of 1968: Geol. Soc. America Spec. Paper 121, p. 557-558.

Sheridan, M.F., and Stuckless, J.S., 1969, volcanics related to the Black Mesa Caldera, central Arizona (abs.), in program with abs. Cordilleran Sec.: Geol. Soc. America abs. with programs, p. 60-61.

Sheridan, M.F., Stuckless, J.S., and Fodor, R.V., 1970, A Tertiary silicic cauldron complex at the northern margin of the Basin and Range Province, central Arizona, U.S.A.: Bull. Volcanol., p. 649-662.

Shieh, Y.N., and Taylor, H.P., 1969, Oxygen and hydrogen isotope studies of contact metamorphism in the Santa Rosa Range, Nevada and other areas: Contr. Mineralogy and Petrology, V. 20, p. 306-356.

Reproduced with permission of the copyright owner. Further reproduction prohibited without permission.

Silver, L.T., 1966, U-Pb isotope relations in Precambrian zircons from Bagdad, Arizona (abs.) in program with abs. meeting Rocky Mountain sec.: Geol. Soc. America abs with programs, p. 62.

Slemmons, D.B., 1962, Determination of volcanic and plutonic plagioclases using a three or four axis universal stage: Geol. Soc. America Spec. Paper 69, 64 p.

Smith, R.L., 1960, Ash flows: Geol. Soc. America Bull, V. 71, no. 6, p. 795-841.

Smith, R.L., and Bailey, R.A., and Ross, C.S., 1961, Structural evolution of the Valles Caldera, New Mexico and its bearing on the emplacement of ring dikes: U.S. Geol. Survey Prof. Paper 424D, p. 145-149.

Stuckless, J.S., 1969, The geology of the volcanic sequence associated with the Black Mesa Caldera, Arizona: Unpub. M.S. Thesis, Arizona State University, 79 p.

Summerhayes, C.P., 1966, Geochronological and strontium isotope study on the Garabal Hill-Glen Fyne igneous complex, Scotland: Geol. Mag., V. 103, p. 153-165.

Tabor, R.W. and Crowder, D.F., 1969, On batholiths and volcanoes - intrusion and eruption of late Cenozoic magmas in the Glacier Peak Area, North Cascades, Washington: U.S. Geol. Survey Prof. Paper 604, 67 p.

Taylor, H.P., and Epstein, S., 1962, Relationship between O^{18}/O^{16} ratios in co-existing minerals of igneous and metamorphic rocks; Part I: Principles and experimental results: Geol. Soc. America Bull., V. 73, p. 461-480.

Taylor, H.P., Jr., 1968, The Oxygen isotope geochemistry of igneous rocks: Cont. Mineralogy and Petrology, V 9, p. 1-71.

Taylor, H.P., Jr. and Epstein, S., 1968, Hydrogen isotope evidence for influx of meteoric ground water into shallow igneous intrusives (abs), in program with abs. annual meeting: Geol. Soc. America abs. with programs, p. 60-61.

Tuttle, O.F., and Bowen, N.L., 1958, Origin of granites in the light of experimental studies in the system $NaAlSi_3O_8$-$KAlSi_3O_8$-$CaAl_2Si_2O_8$-H_2O: Geol Soc. America Mem. 74, 153 p.

Van deKamp, P.C., 1969, Origin of amphibolites in the Beartooth Mountains, Wyoming and Montana: New data and interpretations: Geol. Soc. America Bull., V. 80, p. 1127-1136.

Warren, D.H., 1969, A siesmic-reflection survey of crustal structure in central Arizona: Geol. Soc. America Bull., V. 80, p. 257-282.

Reproduced with permission of the copyright owner. Further reproduction prohibited without permission.

Wilkinson, J.F.G., 1967, The petrology of basaltic rocks; in the Poldevaart Treatis on rocks of basaltic composition, New York, Interscience Publishers, p. 103-162.

Williams, H., Turner, F.J., and Gilbert, C.M., 1959, Petrography: San Francisco, W.H. Freeman and Company, 406 p.

Wilson, E.D., Moore, R.I., and Cooper, J.R., 1969, Geologic Map of Arizona: Arizona Bureau of Mines and U.S. Geol. Survey.

Yoder, H.S., 1971, Contemporaneous rhyolite and basalt: Carnegie Inst. Washington Yearbook 69, p. 141-145.

Reproduced with permission of the copyright owner. Further reproduction prohibited without permission.

Reproduced with permission of the copyright owner. Further reproduction prohibited without permission.

Reproduced with permission of the copyright owner. Further reproduction prohibited without permission.

Reproduced with permission of the copyright owner. Further reproduction prohibited without permission.

Tc
RHYOLITE CONGLOMERATE

Tsc
CANYON LAKE MEMBER
Welded quartz latite tuff. Uppermost member of the Superstition Tuff.

Tsd
DOGIE SPRING MEMBER
Welded quartz latite tuff. Middle member of the Superstition Tuff.

Tss
SIPHON DRAW MEMBER
Welded quartz latite tuff. Lowermost member of the Superstition Tuff.

Tod
OLDER DACITE COMPLEX
Dacite domes, lavas, and autoclastic breccias.

Tob
OLDER BASALTS
Alkali olivine basalts

Ta
ARKOSIC CONGLOMERATE

pCu
pCg
GRANITIC BASEMENT
pCu *Undivided Precambrian*
pCg *Precambrian granitic including the Ruin Granit the Madeira Quartz Diorit*

Reproduced with permission of the copyright owner. Further reproduction prohibited without permission.

EXPLANATION

LITE CONGLOMERATE

Tsc

NYON LAKE MEMBER

d quartz latite tuff.
most member of the
etition Tuff.

Tsd

IE SPRING MEMBER

ed quartz latite tuff
le member of the
etition Tuff.

Tss

IPHON DRAW MEMBER

ed quartz latite tuff.
most member of the
etition Tuff.

Tod

R DACITE COMPLEX

domes, lavas, and
lastic breccias.

Tob

OLDER BASALTS

ali olivine basalts

Ta

ARKOSIC CONGLOMERATE

pCu
pCg

GRANITIC BASEMENT

Undivided Precambrian rocks
Precambrian granitic rocks
luding the Ruin Granite and
Madeira Quartz Diorite.

Tvs

SILICIC VOLCANICS

Undivided silicic volcanics. Largely Geronimo Head Fm. with silicic domes and lavas.

Tydl

QUARTZ LATITE AND RHYOLITE DOMES AND LAVAS

Tgh

GERONIMO HEAD FORMATION

Rhyolite ash-flow tuffs and epiclastic breccias.

YOUNGER BASALTIC LAVAS

Tydl3 *Alkali olivine basalt of Canyon Lake.*
Tydl2 *Basanite of Black Mesa.*
Tydl1 *Alkali olivine basalt of Willow Springs.*

SYMBOLS

Reproduced with permission of the copyright owner. Further reproduction prohibited without permission.

Reproduced with permission of the copyright owner. Further reproduction prohibited without permission.

Reproduced with permission of the copyright owner. Further reproduction prohibited without permission.

Reproduced with permission of the copyright owner. Further reproduction prohibited without permission.

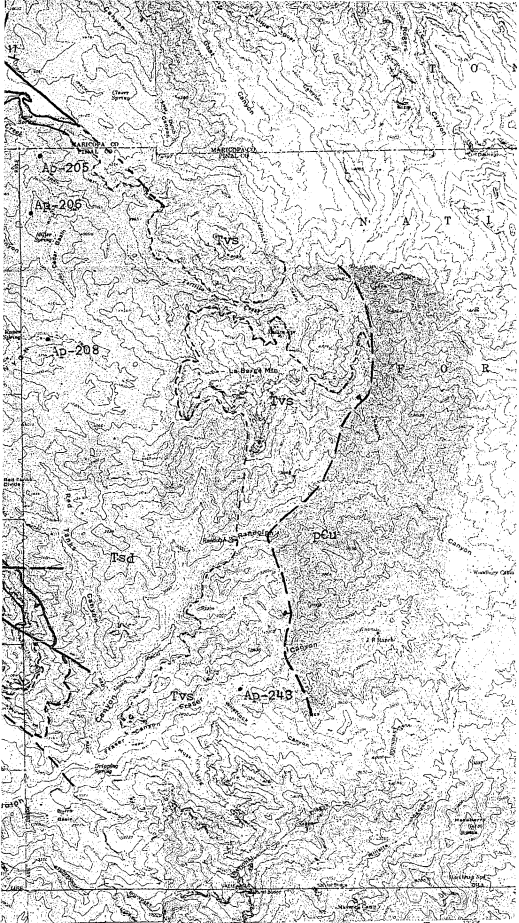

pCu
pCg

GRANITIC BASEMENT

pCu *Undivided Precambrian roc*
pCg *Precambrian granitic rock*
including the Ruin Granite an
the Madeira Quartz Diorite.

geology by J. S. Stuckless, 1971

Reproduced with permission of the copyright owner. Further reproduction prohibited without permission.

GRANITIC BASEMENT

pCu *Undivided Precambrian rocks*
pCg *Precambrian granitic rocks including the Ruin Granite and the Madeira Quartz Diorite.*

SYMBOLS

FAULT

Dot on down-dropped side. Dashed where inferred or approximately located.

CONTACT

Dashed where inferred or approximately located.

18/ ⊕ 18

STRIKE AND DIP OF BEDDING

•Ap-200 •8073

SAMPLE LOCATIONS

Reproduced with permission of the copyright owner. Further reproduction prohibited without permission.

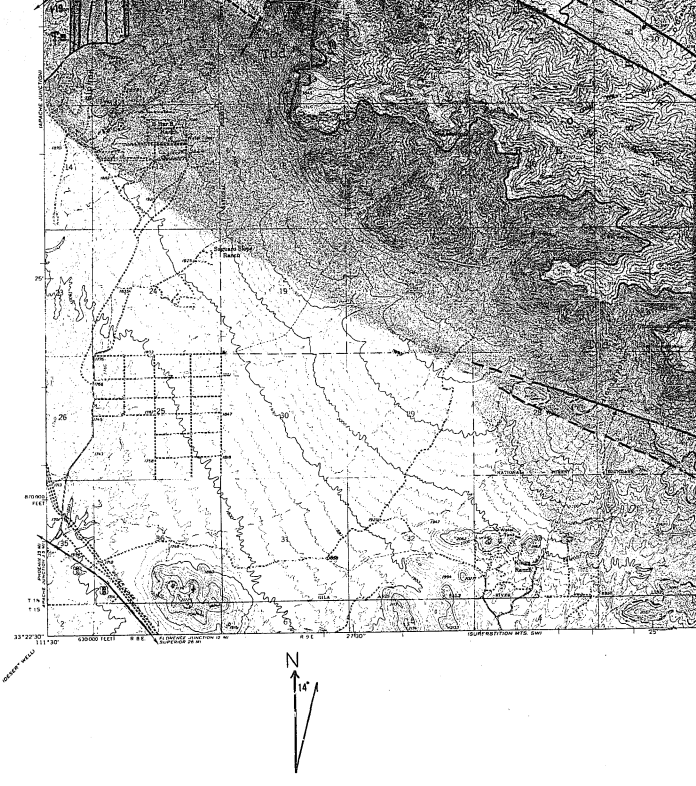

Reproduced with permission of the copyright owner. Further reproduction prohibited without permission.

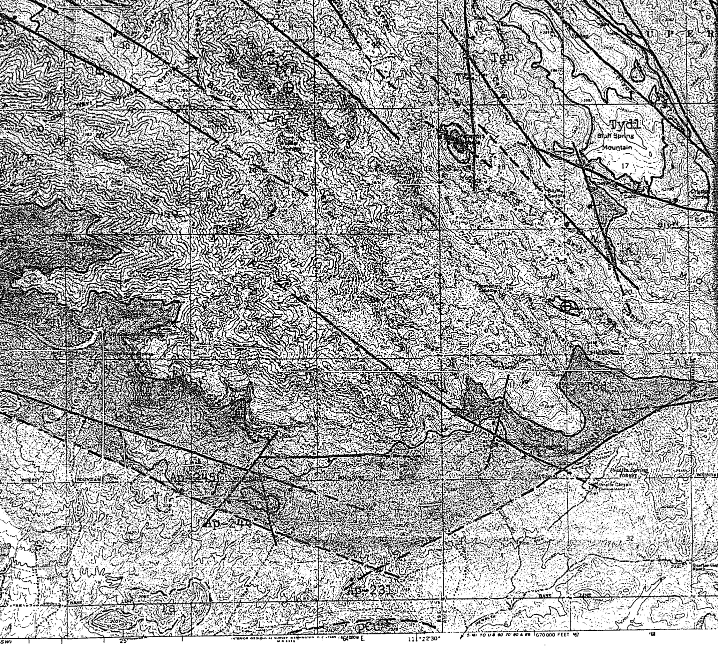

1 0.5 0

1 0.5 0 1 KIL

CONTOUR INTERVAL 20 AND 40 FEE

GEOLOGIC MAP OF THE
MOUNTAIN AREA,

Reproduced with permission of the copyright owner. Further reproduction prohibited without permission.

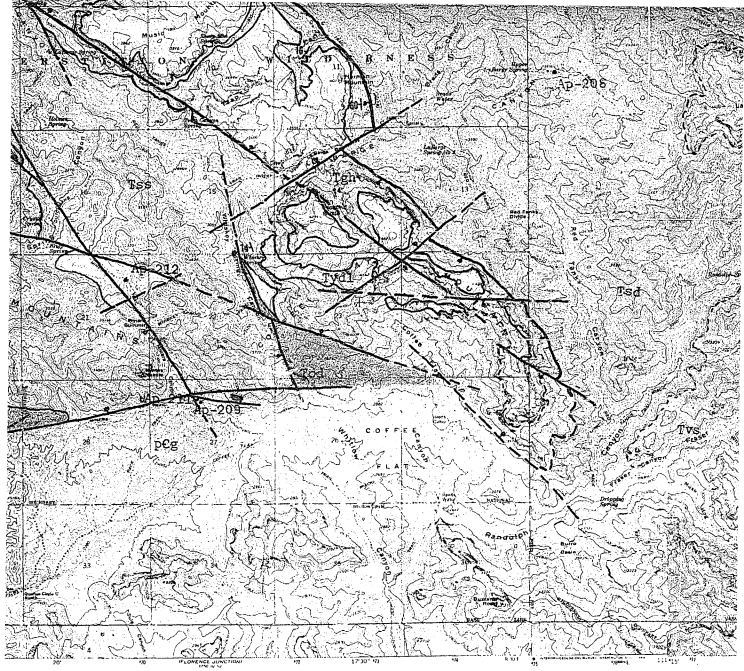

1 MILE

1 KILOMETER

10 FEET

IE SUPERSTITION

A, ARIZONA

Reproduced with permission of the copyright owner. Further reproduction prohibited without permission.

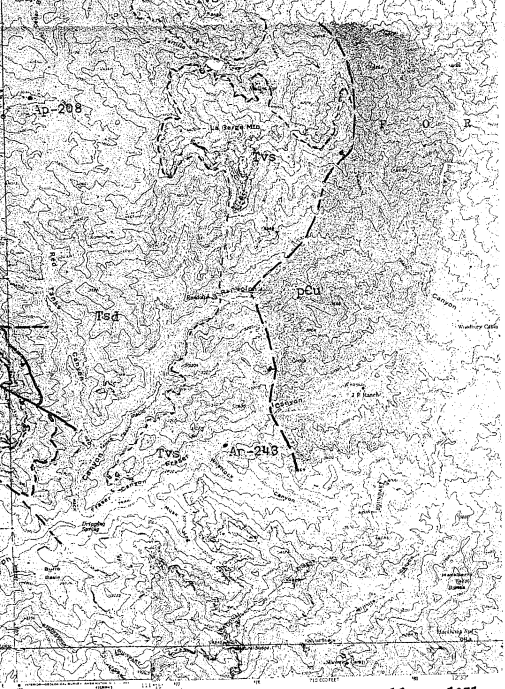

geology by J. S. Stuckless, 1971

Reproduced with permission of the copyright owner. Further reproduction prohibited without permission.